IN-34
141133
P.62

NASA Contractor Report 189737

MODELING AND CONTROL STUDY OF THE NASA 0.3-METER TRANSONIC CRYOGENIC TUNNEL FOR USE WITH SULFUR HEXAFLOURIDE MEDIUM

S. Balakrishna and W. Allen Kilgore

ViGYAN Inc.
Hampton, Virginia

Contract NAS1-18585
December 1992

NASA

National Aeronautics and
Space Administration

Langley Research Center
Hampton, Virginia 23665-5225

Abstract

The NASA Langley 0.3-m Transonic Cryogenic Tunnel is to be modified to operate with sulfur hexaflouride (SF_6) test gas while retaining its present capability to operate with cryogenic nitrogen (N_2) test gas. The modified tunnel will provide high Reynolds number flow on aerodynamic models with two different tunnel test gases. This document details a study of the SF_6 gas tunnel performance boundaries, thermodynamic modeling of the tunnel process, nonlinear dynamical simulation of the mathematical model to yield tunnel responses, tunnel closed loop control requirements, control law generation, and the mechanization of the controls law on the existing tunnel controller.

Nomenclature

A_t	cross sectional area of test section, (0.109 m^2)
A_r	area of recovery valve (normalized)
A_s	area of SF_6 valve (normalized)
b	tunnel circuit loss factor
c	sonic velocity in SF_6, m/s
$\overline{c}$	reference chord for Reynolds number, m
C^*_v	valve flow coefficient
C_p	specific heat of SF_6 at constant pressure, kJ/kg K
C_v	specific heat of SF_6 at constant volume, kJ/kg K
C_m	specific heat of Aluminum 6061, kJ/kg K
C_w	specific heat of water, kJ/kg K
C_h	specific heat of heat exchanger material, kJ/kg K
D	fan tip diameter, m
J	fan advance ratio
K_{cndct}	conduction across heat exchanger, kJ/K s
$K_{( )}$	constants in context
mole	molecular weight, (SF_6 = 146.06, N_2 = 28)
$\dot{m}_t$	test section mass flow, kg/s
$\dot{m}_s$	mass flow of SF_6 into the tunnel, kg/s
$\dot{m}_r$	mass flow returned to the recovery system, kg/s
$\dot{m}_{leak}$	mass flow leaked to the atmosphere, kg/s
$\dot{m}_w$	water flow through the heat exchanger, kg/s

M	Mach number in the test section
M_{fan}	Mach number in fan annuls (one dimensional)
M_{sp}	Mach number set point
n	fan speed, rad/s
N	fan speed, rpm
N_{sp}	fan speed set point, rpm
N_{com}	fan speed command from Mach loop, rpm
P	tunnel total pressure, atm
P_s	static pressure, atm
P_{sf}	SF_6 supply pressure, atm
P_{sp}	pressure set point, atm
P_{st}	SF_6 supply tank pressure (storage), atm
P_b	suction line pressure, atm
q	dynamic pressure, kg/m^2
r	fan pressure ratio
R	universal gas constant, (8.314 kJ/kg-mol K)
$R_{e(\ )}$	Reynolds number for 0.18 m chord
R_{ft}	Reynolds number per foot
s	time, s
S	Laplace operator
t_a	time constant - Mach number, s
t_c	tunnel circuit time, s
t_m	tunnel metal time constant, s
T	total temperature, K
T_s	static temperature, K
T_{sp}	temperature set point, K
T_m	average metal wall temperature, K
T_w	inlet water temperature, K
T_h	average heat exchanger temperature, K
u	velocity, m/s
V	volume of tunnel, m^3
W_g	mass of gas in the tunnel, kg
W_t	mass of metal in the tunnel, (3000 kg)
W_h	thermal mass of heat exchanger, kg
x_r	recovery valve stroke, %

x_S	SF_6 charge valve stroke, %
x_W	water control valve position, %
γ	ratio of specific heats
ρ	density, kg/m^3
λ	skin friction coefficient
μ	viscosity, $N\text{-}s/m^2$
ΔT	fan temperature rise, K
θ	rheostat position for variable frequency generator driving the fan motor, %
ϕ	circular cross section - diameter
κ	concentration of SF_6 (by volume), %
$2\delta h$	gas - water temperature difference in heat exchanger (conduction mode), K

Abbreviations and Some Software Variable Names

ADC	analog to digital converter
AGV	command to nitrogen discharge valves
AISF	command to SF_6 charge valve
ALQ	command to liquid nitrogen valve
ALN	command to liquid nitrogen back pressure valve
AOSF	command to SF_6 recovery valve
AWV	command to water valve
CL	centerline
DAC	digital to analog converter
DACx	voltages from DAC's
DLP	pressure drop across screen/honeycomb in the settling chamber
E( )	voltages to ADC's
IQ	reference voltage signal to variable frequency fan drive Kramer system
HE	heat exchanger
PLQ	liquid nitrogen supply pressure
PSF	SF_6 supply pressure
RSF	SF_6 recovery line pressure
SF_6	sulfur hexaflouride gas
SFCN	concentration of SF_6 (by volume)
SNRP	command voltage signal to fan speed system
TWI	inlet water temperature of heat exchanger
TWO	exit water temperature of heat exchanger

Introduction

Wind tunnel evaluation of scaled aerodynamic models has been the starting point for design of many of the aircraft that have flown since the first flight of the Wright brothers. The Similarity laws of Mach number and Reynolds number have allowed scaling up of subscale model data from wind tunnels to full scale aircraft. The Mach number similarity corresponding to ratio of inertial forces to elastic forces, is easily realized in most wind tunnels. However the Reynolds number similarity which is the ratio of inertial to viscous forces is not easy to realize in small wind tunnels. Lack of this Reynolds number similarity usually introduces errors in test data due to viscosity effects at transonic Mach numbers and when vortex dominated flow or separated flow exists.

The concept of operating a closed circuit wind tunnel with nitrogen gas at cryogenic temperatures is one solution to realize both Mach number and Reynolds number similarities.[1,2] Cryogenic temperature operation of a tunnel with nitrogen gas increases the Reynolds number ($\propto T^{-1.4}$) due to increase in gas density ($\propto T^{-1}$), decrease in viscosity ($\propto T^{-0.9}$). At cryogenic temperatures nitrogen behaves as a perfect gas. In 1973 the NASA 0.3-m Transonic Cryogenic Tunnel (TCT) and later the NASA National Transonic Facility (NTF) were established at Langley Research Center as cryogenic nitrogen gas wind tunnels to conduct high Reynolds number testing on aerodynamic models.

Cryogenic tunnels operate at extremely low temperatures to obtain high Reynolds numbers. These operational temperatures require low temperature qualified instrumentation which are steadily maturing for routine use. Access to the model's on-board instrumentation is not as easy as in ambient temperature tunnels because of the extreme cold. Special procedures are required for servicing the model instrumentation, or the tunnel must be warmed to ambient temperature. In production wind tunnel testing, quick and easy access is considered desirable and therefore alternate methods of realizing high Reynolds numbers in wind tunnels are being pursued.

An alternate method to increase the Reynolds number is to use a high molecular weight gas at ambient temperatures as the tunnel test gas. High gas density and low specific heats ratio is characteristic of some heavy gases like sulfur hexaflouride. This gas has a density about 5.1 times the density of air. This high density yields a high Reynolds number flow at relatively low fan power because of the low specific heats ratio ($\gamma \simeq 1.1$). A sulfur hexaflouride gas tunnel will allow use of ambient temperature force and pressure instrumentation for generating aerodynamic data at high Reynolds number, alleviating many of the low temperature instrumentation problems associated with cryogenic tunnels.

In 1991, a program was started at NASA Langley to modify the 0.3-m TCT to use either cryogenic nitrogen gas or ambient temperature sulfur hexaflouride gas to obtain high Reynolds number flows. Testing an aerodynamic model with both these gases will provide a comparison of high Reynolds number testing from two different gas media. It will also assist in evaluating the validity of sulfur hexaflouride as a wind tunnel test gas with proper perfect gas like thermodynamic properties which may yield true aerodynamic simulation.

Sulfur hexaflouride (SF_6) is an artificially synthesized gas which has been used in the electrical power industry for a number of years because of its high dielectric strength and chemical stability.

The dual gas mode of operation (N_2 and SF_6) for the 0.3-m TCT requires certain design changes to be made to the tunnel circuit and to the control system to precisely control the aerodynamic test parameters in the tunnel flow. The design of closed loop control system for controlling the tunnel flow parameters involves generating an appropriate thermodynamic model to represent the tunnel dynamics. A control and modeling study of the 0.3-m TCT with nitrogen gas was made during the design and commissioning phase of the tunnel control system.[3,4] A new study has now been performed to analyze the tunnel dynamics with SF_6 gas and to redesign the control laws for the modified 0.3-m TCT. In order to generate the dynamical model of the proposed SF_6 tunnel, it is necessary to estimate its performance boundaries. The tunnel performance estimation involves calculation of the new circuit loss pattern, test section mass flow, fan power, fan speed, and other circuit parameters.

This document presents the estimations of the performance limits, the dynamical modeling of the tunnel process, and an analysis of the closed loop control problems using nonlinear dynamical simulation for the proposed 0.3-m TCT with SF_6 gas. This document also presents the necessary control system changes required to operate 0.3-m TCT with SF_6 gas. The controls are expected to hold tunnel pressure to ± 0.07 psia, temperature to $\pm 0.3^\circ$ K and Mach number to ± 0.0015, which will provide the same quality aerodynamic test data as the cryogenic mode of operation.

Thermophysical Properties of Sulfur Hexaflouride

In order to evaluate the dynamics of the tunnel, a study of the basic thermophysical properties of SF_6 gas is necessary. References 5 and 6 detail the properties of SF_6 relevant to this study. This data base has been used to establish the following simplified explicit identities for use in mathematical modeling and analyses. The range of interest for this study is 1 to 6 atm in pressure and 290° to 340°K in temperature, which covers the operating boundaries of the tunnel.

The density of SF_6 can be approximated as:

$$\rho = 1842 \left(\frac{P}{T} + 0.193 \left\{ \frac{P}{T} \right\}^2 \right) \qquad \mathrm{kg/m^3}$$

The density of SF_6 gas is about 5.1 times higher than air. A plot of the SF_6 density as a function of pressure and temperature is shown in figure 1.

The specific heat at constant pressure for SF_6 can be expressed as an approximate function of temperature and pressure as:

$$C_p = 221 + 35.01\ P + (1.49 - 0.09\ P)\ T \qquad \mathrm{J/kg\ K}$$

A plot of the SF_6 specific heat at constant pressure is shown in figure 2.

Obviously, SF6 does not behave like a perfect gas since C_p is a function of pressure. However a γ can be defined as the specific heat ratio as:

$$\gamma = 1.1415 - 0.000167\ T + P\ (0.02748 - 0.0000735\ T)$$

A plot of the SF_6 specific heat ratio is shown in figure 3.

The specific heat at constant volume can be established from the above two identities as:

$$C_V = \frac{C_P}{\gamma} = \frac{221 + 35.01\ P + (1.49 - 0.09\ P)\ T}{1.1415 - 0.000167\ T + P\ (0.02748 - 0.0000735\ T)} \qquad \text{J/kg K}$$

The viscosity of SF_6 is a function of temperature and can be expressed as:

$$\mu = 5.49\ (T - 14.34)\ 10^{-8} \qquad \text{N-s/m}^2$$

The following isentropic relations, with real γ, have been used throughout this analysis to represent SF_6 gas states as it flows through the contraction and other segments of the tunnel. It should be pointed out that use of real γ in isentropic relations is not strictly valid due to real gas effects such as the imperfect thermal and caloric properties of the gas.

$$P_S = \frac{P}{\left(1 + \frac{(\gamma-1)}{2} M^2\right)^{\frac{\gamma}{\gamma-1}}} \qquad\qquad T_S = \frac{T}{\left(1 + \frac{(\gamma-1)}{2} M^2\right)}$$

Sulfur Hexaflouride Tunnel Operation

The schematic diagram of the modified 0.3-m TCT circuit for use with SF_6 gas is shown in figure 4. It is proposed to work the tunnel with a SF_6 gas purity of about 98%, since dilution with air is probable in charging and recovering the gas. The first charge of SF_6 into the tunnel shell is preceded by evacuation of the tunnel resident air to a near vacuum. The tunnel pressure is built up by injecting the SF_6 gas derived from liquid storage. A boiler/evaporator is used to generate SF_6 gas from the liquid SF_6 at a source pressure of about 200 psig. A pressure reducer-regulator maintains the source supply pressure to the injection valve. This source is used to control the gas mass flow into the tunnel through the proportional control valve 3914R. Since SF_6 is costly and is not a natural gas in the atmosphere, it is not desirable to release the gas to the atmosphere. Hence, the gas is confined to a close loop cycle of vaporization, recovery, and liquefaction. Therefore, the tunnel pressure is decreased by removing the gas into a recovery system. The control valve 3900R delivers recovery gas into the compressor of a recovery system. This recovery system liquefies SF_6 gas through a refrigeration system and the resultant liquid SF_6 is stored for reuse. Therefore, two different valves are used for SF_6 tunnel pressure control, one for increasing and the second for decreasing tunnel resident gas mass.

The operation of the tunnel fan results in an increase of tunnel gas temperature because of adiabatic compression due to the work done by the fan. To regulate the gas temperature, a heat exchanger will be used in the low-velocity, diffuser segment of the tunnel. The heat exchanger uses cooling water flow through control valve 3441U for removing the heat from tunnel gas. In the cryogenic mode of operation, liquid nitrogen performs the cooling function, hence a heat exchanger is not required. The heat exchanger will be made using material compatible to cryogenic operation down to 78 K, allowing it to remain in the tunnel circuit during cryogenic mode operation. Provision has been made to allow draining and drying of the water lines that will be exposed to cryogenic temperatures. The heat exchanger introduces extra circuit losses and extra metal mass in the externally insulated tunnel circuit. The issues involved in sizing the heat exchanger and its impact on the tunnel Reynolds number are also considered in this study. The fan speed requirement for operating the SF_6 mode tunnel is a function of tunnel geometry and the fan advance ratio and is estimated in this study.

The tunnel flow Mach number is controlled by a variable speed motor driving the fan. The fan rotation creates the necessary pressure ratio for realizing a desired velocity in the test section. The fan has fixed guide vanes and is surge free for the envelope of tunnel operations. The fan is driven by a variable speed 2 pole squirrel cage AC induction motor capable of nearly 7200 rpm where it can deliver a maximum power of 2240 kw. Because of the high density of SF_6 gas the maximum fan speed required in the SF_6 mode is expected to be less than 2800 rpm.

Tunnel Circuit Variables

Using the isentropic flow relations, the approximate test section mass flow can be expressed as:

$$\dot{m}_t = \rho u A_t = 1842 \sqrt{\frac{R\gamma}{mole}}\, A_t \frac{P\ M}{\sqrt{T}\left(1+\frac{(\gamma-1)}{2}M^2\right)^{\frac{(\gamma+1)}{2(\gamma-1)}}} \quad \text{kg/s}$$

with $u = c\,M = \sqrt{\frac{R\gamma T_S}{mole}}\,M$ (approximately $7.95\,M\,\sqrt{T_S}$ m/s for $\gamma = 1.1$)

A plot of the test section mass flow, covering the operational envelope of the tunnel, is shown in figure 5 as a function of total temperature and total pressure.

Consider a case when the tunnel is charged to a uniform pressure P, under no flow conditions. Once the tunnel fan is started, the static pressure in the test section reduces from the original value of P, thereby reducing the mass of gas in the test section. The excess mass is redistributed to the rest of the tunnel and hence the total pressure P, increases as a function of Mach number. This change in tunnel pressure is a function of the tunnel geometry and can be obtained by adding mass in each segment as a function of test section Mach number and the plenum volume, as shown in Table 1. This has been estimated as,

$$W_g = 1842 \int^{circuit} \frac{P_S}{T_S}\,dV \simeq 1842\,\frac{P\,V}{T}\,(1 - 0.033\,M^2) \qquad \text{0.3-m TCT-specific identity}$$

The tunnel circuit time is the time taken for a molecule to go around the closed circuit once in the sense of a one dimensional flow. Ignoring the plenum volume, the tunnel circuit time can be estimated and is shown in figure 6.

$$t_c = \frac{W_g}{\dot{m}_t}$$

The tunnel test section Reynolds number can be estimated by using expressions for density ρ, viscosity μ, and velocity u as:

$$R_{e(SF_6)} = \frac{\rho\,u\,\overline{c}}{\mu} = \frac{1842}{5.49}\sqrt{\frac{R\gamma}{mole}}\,\frac{P_S\,M\,\overline{c}}{\sqrt{T_S}\,(T_S - 14.34)}\,10^8$$

$$\simeq 267710\,\frac{P_S\,M\,\overline{c}}{\sqrt{T_S}\,(T_S - 14.34)}\,10^6 \text{ for } \gamma = 1.1$$

Figure 7 shows the Reynolds number envelope of the tunnel for a 0.18 m chord aerodynamic model. The envelope shows the fan power limit imposed by the existing motor and the Kramer speed control drive system at 0.3-m TCT. The figure also shows the loci of candidate heat exchanger design limits based on the capacity of the heat exchanger. These loci are useful in optimizing the heat exchanger circuit loss during the initial design trade-off studies.

The test section Reynolds number changes when the SF_6 gas is diluted by other gases, and for a given concentration of SF_6 of κ (by volume) assuming dilution only by air:[5]

$$R_{e(mix)} = \left\{1 - 0.00699\ (100-\kappa)\right\} R_{e(SF_6)} \qquad \text{for } 90 < \kappa < 100\ \%$$

Tunnel Geometry, Circuit Losses, and Fan Power

The 0.3-m TCT geometrical details for the proposed modifications for SF_6 operation are shown in Table 1. Details of the eleven segments constituting the closed circuit tunnel with their cross section, length, volume, local Mach number (when test section is at Mach 1) and the circuit loss factor are presented.

Table 1

Tunnel segment	Cross section mϕ or area	Length m	Volume m^3	M_{local} (M_{test}=1.0)	Loss $\frac{\Delta p_{sea}}{q_{test\ sec}}$
Fan nacelle/vanes	0.762	4.05	1.67	0.1448	0.009
HE inlet diffuser	0.762-0.978	2.44	1.43	0.111	
Rapid diffuser to HE	0.978-1.22	0.41	0.39	0.066 av	
Heat Exchanger	1.22	0.92	1.067	0.0560	0.025
HE exit diffuser	1.22	1.22	1.422	0.0560	
Bigend corners/crossleg	1.22	3.29 CL	4.00	0.0560	0.005
Settling chamber/screen	1.32	1.75	2.40	0.0464	0.004
Contraction	1.32 ϕ-0.109 m^2	1.27	0.579	0.1559 av	0.009
Test section*	0.109 m^2	1.93	0.210	1.00	0.040
High speed diffuser	0.109m^2-0.762	4.88	0.99 m^3	0.4716 av	0.054
1 & 2 corners/crossleg	0.762	3.35 CL	1.52 m^3	0.1448	0.014
Fan annulus	0.762/0.413	1.00	0.5 m^3	0.2072	-
Total		26.51 CL	16.18 m^3		0.160

* The plenum pressure volume of 0.6 m^3 (not participating in flow) is not included

The test section plenum volume of about 0.6 m^3 is connected to test section pressure to prevent pressure loading across the flexible walls, and is treated as a pressure volume but not a flow volume. The local flow Mach number in each segment of the tunnel has been estimated using the continuity equation starting from the mass flow and local cross sectional area. The real value of γ for SF_6 has been used in the estimation.

$$\frac{M}{\left(1+\frac{(\gamma-1)}{2}M^2\right)^{\frac{(\gamma+1)}{2(\gamma-1)}}} - \frac{\dot{m}_t \sqrt{T}}{1842 \sqrt{\frac{R\gamma}{mole}}\, P\, A} = 0$$

This equation has been solved for the given mass flow, total pressure, and temperature at various cross sectional areas along the tunnel center line to arrive at the local one dimensional flow Mach number. The tunnel circuit loss factor has been estimated segment by segment and normalized to the test section dynamic pressure. These estimates are based on procedures detailed in reference 7. A skin friction coefficient of λ=0.007 (for average Reynolds numbers of 30 million/diameter on internal surface) has been assumed for the calculations.

The heat exchanger is design is based on a nominal allowable flow pressure loss across the heat exchanger of 0.70 psi at P=6 atm and M=0.8. This corresponds to a circuit loss factor of 0.025.[8] The loss factor due to heat exchanger is inversely proportional to the design value of the water-gas temperature difference allowed at maximum power. Reducing this temperature difference results in higher tunnel circuit loss factors. The heat exchanger circuit loss from the present design choice accounts for 16-18% of the total tunnel circuit losses. In the settling chamber, the screen losses are assumed to be about 1 to 2 times the local dynamic pressure.

The dominant circuit losses appear to occur in the high speed diffuser, the test section and the heat exchanger. The fan pressure ratio for steady state operation at test section Mach number M is:

$$r = 1 + bM^2 \quad \text{where } b = 0.160$$

The 0.3-m TCT circuit losses under cryogenic operation have been estimated and quantified.[9] In reference 9, the fan pressure ratio in the cryogenic mode of operation was extensively measured and analyzed during the early 1980's. The fan pressure ratio was curve fit as a function of the test section Reynolds number R_{ft}. Using the expression from reference 9, the 0.3-m TCT circuit loss factor can be estimated for a typical Reynolds number of about 50-60 million/foot as:

$$r = 1.001 + 0.8205\, M^2\, R_{ft}^{-0.096} \simeq 1 + 0.150\, M^2$$

This circuit loss factor of 0.150 (*Circa 1984*) was lowered with the introduction of a smaller 0.109 m^2 test section and the new improved diffuser (*Circa 1986*). Assuming 7-8% improvement due to these changes, the unmodified tunnel circuit loss can be estimated at 0.138. This circuit loss factor is consistent with the present estimate of circuit losses for the modified configuration of 0.160 at 50 million/foot Reynolds number. The loss factor of 0.160 accounts for the inclusion of the new heat exchanger, and modification of the old, low-speed diffuser duct. The modified tunnel fan pressure ratio can be expressed as:

$$r = 1.001 + 0.8765\, M^2\, R_{ft}^{-0.096} \simeq 1 + 0.160\, M^2$$

After the tunnel modifications for the SF_6 mode, future cryogenic operation will include the extra circuit losses due to the new heat exchanger. Hence, the performance envelope of the cryogenic mode is likely to change. The fan power consumption for a tunnel circuit with known circuit loss factors can be estimated using the fan temperature ratio by invoking isentropic relations. Since cooling occurs after compression, the fan outlet temperature is T+ΔT, and hence:

$$r = \left(\frac{T + \Delta T}{T}\right)^{\frac{\gamma}{\gamma-1}} = 1 + b\, M^2$$

$$\Delta T = T\left\{\left(1+bM^2\right)^{\frac{\gamma-1}{\gamma}} - 1\right\} \simeq 0.94\, T\, b\, M^2\, \left(\frac{\gamma-1}{\gamma}\right)$$

$$\text{Fan power} = \dot{m}_t\, C_p\, \Delta T \simeq K_f \frac{P\, M^3 \sqrt{T}}{\left(1+\frac{(\gamma-1)}{2}M^2\right)^{\frac{(\gamma+1)}{2(\gamma-1)}}}$$

$$\text{where } K_f = 1842 \sqrt{\frac{R\gamma}{\text{mole}}}\, A_t\, C_p\, \left(\frac{\gamma-1}{\gamma}\right) b$$

Figure 8 shows the fan power as a function of tunnel Mach number and pressure. In estimating the power, a constant value for b has been assumed. Value of b varies with tunnel flow Reynolds number, but its effect has been ignored. Figure shows the speed based power limit on the 2240 kw, 7200 synchronous rpm water-cooled, squirrel-cage 2-pole induction motor, working at 35 V rms/Hz, which limits the performance envelope of the tunnel from an operational point of view. The effect of the fan power limitation and the heat exchanger capability, as a set of power loci, on the tunnel Reynolds number is illustrated in figure 7. The heat exchanger and its cooling water temperature determine the maximum fan power that can be used while still retaining the ability to regulate tunnel total temperature.

Fan Speed

The 0.3-m TCT fan has twelve blades with seven fixed inlet and outlet guide vanes. The fan pressure ratio is controlled by the fan runner speed. The fan advance ratio, as existing, is estimated for cryogenic nitrogen operation from a recorded case.[4] The tunnel was operated at M=0.760, P=68 psia, and T=230 K, and the resulting fan speed was found to be 4504 rpm. For this test the tunnel had a Cast-10 model in the test section and the flexible walls were streamlined. The fan tip diameter is 0.762 m and the fan boss diameter is 0.413 m. From these data, the fan annulus one dimensional flow Mach number is estimated as 0.189 by solving the mass flow equation with nitrogen molecular weight of 28, specific heat ratio γ of 1.4, and density of 338.9 $\frac{P}{T}$. The fan advance ratio is:

$$J = \frac{u}{nD} = \frac{c\,M_{fan}}{n\,D} = \left\{ \frac{\sqrt{\frac{R\gamma}{mole}\,T_s}\;M_{fan}}{\pi\,\frac{N}{60}\,D} \right\} = 0.3083$$

By assuming that the flow rotation imparted by the fan to be negligible, the fan advance ratio J can be considered as an invariant parameter of the tunnel applicable for both test gases. Utilizing the J estimated from the cryogenic nitrogen mode, the mass flows and local Mach numbers around the circuit can be determined for the SF_6 mode.

Table 2

Temperature = 311 K, Pressure = 6 atm

Test section $\dot{m}_t$, kg/s	Test section Mach no.	Fan annulus Mach no.	Fan speed rpm
323	0.96	0.2072	2349
320	0.89	0.2048	2322
315	0.835	0.2014	2284
310	0.795	0.198	2246
300	0.733	0.1915	2172
290	0.6838	0.1848	2096
280	0.6414	0.1782	2021
240	0.5079	0.1521	1726
200	0.4027	0.1263	1433
161	0.3152	0.1018	1155
120	0.228	0.0753	855
80	0.1497	0.0501	569
40	0.0742	0.025	283

The relation between the test section Mach number and the fan annulus Mach number is nonlinear. Table 2 provides the tunnel mass flow and corresponding test section Mach number/fan annulus Mach number, and, finally the estimated fan speed for the SF_6 test gas. This table has been obtained by solving the continuity equation for a given tunnel mass flow, temperature, and pressure for at the test section and the fan annulus areas (test section 0.109 m^2 and fan annulus of 0.762 m tip diameter and 0.413 m boss diameter).

$$\frac{M}{\left(1+\frac{(\gamma-1)}{2}M^2\right)^{\frac{(\gamma+1)}{2(\gamma-1)}}} - \frac{\dot{m}_t\sqrt{T}}{1842\sqrt{\frac{R\gamma}{mole}}\ P\ A} = 0$$

$$N = \frac{60\sqrt{\frac{R\gamma}{mole}T_s}\ M_{fan}}{\pi\, J\, D}$$

Figure 9 shows the fan speed as a function of Mach number. It is basically independent of tunnel pressure. Under steady state conditions, the fan speed Mach number relation can be expressed as (using a quadratic regression curve fit):

$$\frac{N}{\sqrt{T}} = 251\ M\ (1\ -\ 0.474\ M)$$

The fan imparts a momentum increase to the flow which provides the test section Mach number M. The 0.3-m TCT has solid adaptive wall system, and hence tunnel flow does not breathe into the plenum in a dominant manner as in a slotted or porous wall test section. The dynamics of the Mach number can be expressed as:

$$\frac{dM}{dt} = \frac{1}{K_n}\frac{N}{t_a\sqrt{T}} - \frac{M}{t_a} \qquad \text{where } K_n = 251\ (1\ -\ 0.474\ M)$$

The fan drive electrical system, consists of a field-controlled DC generator driving a DC motor coupled to a variable frequency alternator. The transfer function of whole system is:[3]

$$\frac{N}{N_{sp}} = \frac{1}{1 + 0.56\ S + 0.2\ S^2}$$

This transfer function model was experimentally determined from time response records of the fan speed perturbation during cryogenic tunnel operation.

The low fan speed requirement for SF_6 limits the amount of power that can be derived from the fan based on motor current limitation. The motor can deliver a maximum power of 31.1 kw/100 rpm. This limits the SF_6 tunnel performance boundary as already discussed and illustrated in figure 8.

Tunnel Pressure and Temperature Dynamics

In order to operate a closed circuit tunnel with SF_6, mass flow into and out of the tunnel is necessary to incorporate pressure control feature. The operation of the fan results in adiabatic compression of gas and the heat from compression is released into the tunnel gas. Mass enthalpy interaction occurs continuously in the tunnel, affecting the tunnel pressure and temperature states. The dynamics of this interaction can be studied using the equations of state, energy, continuity, heat transfer from tunnel metal shell to gas, heat transfer from gas to cooling water through the heat exchanger, adiabatic compression heat release, a simple, surge-free fan map, and a few related identities based on the thermophysical properties of the gas. The SF_6 inlet mass flow, $\dot{m}_s$, recovery flow, $\dot{m}_r$, cooling water mass flow, $\dot{m}_w$, and fan speed, N, are used to control the tunnel states to desired values. In the lumped modeling approach, the mass enthalpy interactions are assumed to control the average tunnel state and, hence, the total pressure and temperature in the settling chamber. In this model, the spatial distribution of the total gas states around the circuit is based on the average state less local losses, except for the segment between the fan and the heat exchanger. From the ideal gas equation of state, the pressure rate in the tunnel can be expressed as:

$$\frac{dP}{dt} = \frac{P}{T}\frac{dT}{dt} + \frac{P}{W_g}(\dot{m}_s - \dot{m}_r - \dot{m}_{leak})$$

The energy components in the tunnel are from enthalpy movement in and out of the tunnel due to SF_6 gas mass charging-recovery, adiabatic compression of the tunnel gas flow at the fan, tunnel metal wall to gas convection heat transfer, and the heat transfer in the heat exchanger from gas to heat exchanger body mass. The temperature rate in the tunnel can be expressed as:

$$\frac{dT}{dt} = \frac{1}{W_g C_v}\left\{K_f P \frac{M^3\sqrt{T}}{\left(1+\frac{(\gamma-1)}{2}M^2\right)^{\frac{(\gamma+1)}{2(\gamma-1)}}} + (\dot{m}_s - \dot{m}_r - \dot{m}_{leak})\, C_p T \right.$$
$$\left. - W_t C_m \frac{T-T_m}{t_m} - C_p \dot{m}_t\left(T + \frac{\Delta T}{2} - T_h - \delta h\right)\right\}$$

The heat exchanger heat transfer involves the interaction between gas mass flow, heat exchanger body conductivity, and water mass flow. Under steady state tunnel conditions, the SF_6 gas inlet total temperature to the heat exchanger is $T+\Delta T$ and the gas exit temperature is T. Therefore the average gas temperature in the heat exchanger is $(T+\frac{\Delta T}{2})$. The heat transfer from gas to water involves conduction through the tube walls and a change in the heat exchanger body mass temperature. T_h is the average heat exchanger body mass temperature, the gas side surface temperature is $T_h+\delta h$ and water side surface temperature is $T_h-\delta h$, the temperature difference across the tube walls is $2\delta h$. This temperature difference across tube wall accounts for conduction mode heat transfer from gas to water. The difference between heat entering and leaving the heat exchanger dictates the heat exchanger body temperature dynamics. The heat exchanger metal mass thermal dynamics can now be determined as:

$$W_h C_h \frac{dT_h}{dt} = C_p \dot{m}_t \left\{T + \frac{\Delta T}{2} - (T_h + \delta h)\right\} - C_w \dot{m}_w \left\{(T_h - \delta h) - T_w\right\}$$

The quantum of heat entering the heat exchanger in the conduction mode is a function of the temperature difference across the heat exchanger tube walls $2\delta h$.

$$\frac{1}{2}\left\{C_p \dot{m}_t \left(T + \frac{\Delta T}{2} - T_h - \delta h\right) + C_w \dot{m}_w (T_h - \delta h - T_w)\right\} = K_{cndct}(2\delta h)$$

The temperature difference between the gas and water sides of the heat exchanger can be determined by simplifying the above expression.

$$\delta h = \frac{1}{4K_{cndct} + C_p \dot{m}_t + C_w \dot{m}_w} \left\{C_p \dot{m}_t \left(T + \frac{\Delta T}{2} - T_h\right) + C_w \dot{m}_w (T_h - T_w)\right\}$$

From the design data (based on 5.2° K temperature rise of 32 kg/s, 291.5° K water flow with tunnel at 319.4 K, M=0.8 P=6 atm), K_{cndct} for the heat exchanger is estimated as 29 kJ/s K. [8]

The time constants associated with heat transfer from the gas to the heat exchanger vary as a function of tunnel mass flow $\dot{m}_t$. Typically, under equilibrium conditions, the fan raises the gas stream temperature by ΔT and the heat exchanger cools the stream back to T. The quantum of heat removed by water flow equals the heat exchanger heat flow. The water-gas heat exchanger is made of finned copper tubing and its thermal mass is dominated by copper whose specific heat is:[8]

$$C_h = 385.4 \text{ J/kg K}$$

The water flow throttling control valve is located downstream of the heat exchanger and uniformity of the temperature is not expected to be as good as when a constant mass flow, variable water inlet temperature concept is used for the heat exchanger as in the NTF.

The 0.3-m TCT is an externally insulated tunnel made out of Aluminum 6061 which has a specific heat which varies with temperature as:

$$C_m = (5.5\ T\ -\ 0.008\ T^2)\ J/kg\ K$$

The tunnel metal wall to gas heat exchange can be expressed by the identity:

$$\frac{dT_m}{dt} = \frac{(T\ -\ T_m)}{t_m}$$

The tunnel gas to metal heat transfer is a function of gas density and convection rate occurring at the turbulent boundary layer throughout the internal surface of the tunnel due to the motion of the gas along the walls. This has been formed as a time constant that is inversely proportional to mass flow $\dot{m}_t$ and has been experimentally validated in the cryogenic mode of operation as:

$$t_m = \frac{K_m}{T^{0.12}\ (P\ M)^{0.8}}\ \ s \qquad\qquad \text{0.3-m TCT-specific identity}$$

Sulfur Hexaflouride Mass Flow Control

The mass flow of the SF_6 gas into the tunnel and out to the recovery system is controlled by proportional control valves. The valve stroke-area is modeled to have a 2% dead band near zero a with nonlinear stroke-area law. The inlet to the tunnel is controlled by one of the unused liquid nitrogen injection valves with a full open valve coefficient C^*_v of 14. For SF_6 at a density ratio of 5.1, the mass flow in to the tunnel can be expressed as.

$$\dot{m}_s =\ 0.1811\ \frac{P_{sf}}{\sqrt{T}}\ C^*_v\ \ \ kg/s \qquad\qquad \text{choked flow}$$

However, in the proposed design the maximum rate of evaporation from the SF_6 boiler/evaporator is limited to 0.274 kg/s. The inlet valve is oversized for this mass flow, requiring only a partial opening to generate the full mass flow. The maximum opening can be limited in the control software appropriately.

Sulfur hexaflouride gas is recovered through a recovery system with a compressor/liquefaction unit. The compressor suction line is connected to the tunnel exhaust through a proportional control valve with a full open valve coefficient C^*_v of 7.8. Depending upon the tunnel operating pressure, the flow through this valve can be either choked or unchoked. The equations for mass flow removal are:

$$\dot{m}_r = 0.1811 \frac{P}{\sqrt{T}} C^*_v \quad \text{kg/s for } P > 1.5\, P_b \text{ (choked flow)}$$

$$\dot{m}_r = K_{r1}\sqrt{\frac{P}{T}(P - P_b)} \; C^*_v \quad \text{kg/s for } P < 1.5\, P_b \text{ (unchoked flow)}$$

$$\dot{m}_{leak} = 0.02786 \frac{P}{\sqrt{T}} \quad \text{kg/s for } P > 1.5 \text{ atm (equivalent to 0.1 inch diameter orifice)}$$

The proposed compressor for the recovery system has a maximum capability of 0.137 kg/s mass flow.[8] A valve of C^*_v=7.8 has been used to provide a fine resolution and closed loop control for low mass flows at higher pressure loss. Another valve of C^*_v=10 is used in parallel under openloop control during shutdown to evacuate tunnel and store the SF_6 gas rapidly.

Control Laws

The tunnel dynamics are highly coupled and nonlinear in nature. The SF_6 medium tunnel does not have complex dynamical modes and the control problem is basically one of quasi-statically balancing the nonlinear energy terms through the control inputs. Since the mass enthalpy control terms are relatively small, the tunnel response time tends to be very slow. In order to obtain good quality aerodynamic data, the stability criteria in tunnel control is to control pressure to ± 0.007 psia, temperature to $\pm 0.3^\circ$ K and Mach number to ± 0.0015 of the set point values. The control laws are developed from analysis and nonlinear simulation and are discussed in the following sections.

The tunnel gas temperature control is realized by cooling water mass flow control under closed loop control. The basic equations which control the tunnel gas temperatures are:

$$\frac{dT_m}{dt} = \frac{(T-T_m)}{t_m}$$

$$\frac{dT}{dt} = \frac{1}{W_g C_v}\left\{K_f \frac{P\, M^3 \sqrt{T}}{\left(1+\frac{(\gamma-1)}{2}M^2\right)^{\frac{(\gamma+1)}{2(\gamma-1)}}} + (\dot{m}_s - \dot{m}_r - \dot{m}_{leak})C_p T - W_t C_m \frac{T-T_m}{t_m} - C_p \dot{m}_t (T + \frac{\Delta T}{2} - T_h - \delta h)\right\}$$

$$\frac{dT_h}{dt} = \frac{1}{W_h C_h}\left\{ C_p \dot{m}_t \,(T+\frac{\Delta T}{2} - T_h - \delta h) - C_w\, \dot{m}_w (T_h - \delta h - T_w)\right\}$$

$$\delta h = \frac{1}{4K_{cndct} + C_p \dot{m}_t + C_w \dot{m}_w}\left\{C_p \dot{m}_t \,(T + \frac{\Delta T}{2} - T_h) + C_w\, \dot{m}_w (T_h - T_w)\right\}$$

The model is nonlinear for the temperature control variable $\dot{m}_w$, and hence control law synthesis using classical linear control methods are not feasible. The control law has been established through dynamic simulation. For a temperature set point T_{sp}, the control law will be gain scheduled as a function of tunnel mass flow, which dictates the rate of heat removal.

$$\dot{m}_w = \frac{\dot{m}_t}{70}\left\{(T - T_{sp}) + 0.1 \int (T - T_{sp})\right\} \qquad 0 < \dot{m}_w < 32 \text{ kg/s}$$

or as valve position, the control law will be:

$$x_w = \frac{\dot{m}_t}{23}\left\{(T - T_{sp}) + 0.1 \int (T - T_{sp})\right\} \qquad 0 < x_w < 100\ \%$$

where 0% command corresponds to 4 milliamperes and 100% command corresponds to 20 milliamperes drive for the pneumatically driven valve positioner. A linear flow-current transfer function has been assumed for the modeling of mass flow. A small dead band type nonlinearity exists in most valves followed by a nonlinear area-stroke relationship. This nonlinear area-stroke model will be introduced in the nonlinear dynamical simulation to study the performance of the tunnel.

The total pressure control equation for the tunnel is:

$$\frac{dP}{dt} = \frac{P}{T}\frac{dT}{dt} + \frac{P}{W_g}(\dot{m}_s - \dot{m}_r - \dot{m}_{leak})$$

The control variables in the above equation are $\dot{m}_s$ for pressure increase and $\dot{m}_r$ for pressure decrease. Hence two separate valves (C^*_v=14 for the charging valve and C^*_v= 7.8 for the recovery valve) will be used for bipolar control. The pressure control dynamics are nonlinear with coupling from the temperature control loop. Again, through simulation, to be discussed in the next section, the pressure control law has been formulated as:

$$x_s = 10\left\{(P_{sp} - P) + 0.03\int(P_{sp} - P)\,dt\right\} \quad \text{where } 0 < x_s < 100\%$$

$$\dot{m}_s = 0.2535\,\frac{P_{sf}}{\sqrt{T}}\,A_s \quad \text{where } A_s = 0 \text{ for } 0 < x_s < 2 \text{ and } A_s = \left(\frac{x_s}{100}\right)^{1.7} \text{ for } 2 < x_s < 100$$

At about 10 atm infinite volume source pressure, the full open mass flow will be 2 kg/s. However, the maximum boiling rate of the supply system is 0.274 kg/s and hence, to obtain linear mass flow control, the maximum charge valve opening may have to be limited to 15 - 20% for linear control.

$$x_r = 10\left\{(P_{sp} - P) + 0.03\int(P_{sp} - P)\,dt\right\} \quad \text{where } 0 < x_r < 100\%$$

$$\dot{m}_r = 0.1811\,\frac{P}{\sqrt{T}}\,A_r \quad \text{where } A_r = 0 \text{ for } 0 < x_r < 2 \text{ and } A_r = \left(\frac{x_r}{100}\right)^{1.7} \text{ for } 2 < x_r < 100$$

These two control laws work in tandem on each valve driving the position on the basis of 4 to 20 milliamperes drives for the pneumatically operated valve positioners. The valve stroke-area is modeled to be a 2% dead band with nonlinear area law.

The tunnel Mach number control is essentially same as the control law discussed in reference 4, and is based on the fan speed Mach number relation of:

$$\frac{N}{\sqrt{T}} = 251\ M\ (1\ -\ 0.474\ M)$$

The tunnel is on a fan speed control loop where the rheostat driving the variable frequency generator is adjusted by the control law:

$$\theta = 0.6\ (\ N - N_{sp}) + \int (N - N_{sp})\ dt$$

where θ and $\left|\int (N - N_{sp})\ dt\right|$ are limited in each computation such that maximum fan acceleration/deceleration is less than 50 rpm/s.

For closing the Mach number control loop, the test section Mach number is estimated from the total and static pressures from isentropic relations as:

$$M = \sqrt{\frac{2}{\gamma\text{-}1}\left\{\left(\frac{P}{P_s}\right)^{\frac{2(\gamma\text{-}1)}{(\gamma+1)}} - 1\right\}} \quad \text{when } \gamma\text{=}1.1, \quad M = \sqrt{20\left\{\left(\frac{P}{P_s}\right)^{\frac{1}{10.5}} - 1\right\}}$$

In the control laws, the value of γ is estimated from the measured P and T. The Mach number control law generates the fan speed command using only a proportional law. An integration in the Mach number control loop would result in a double integration in the fan speed control loop, leading to an undesirable overshoot. Hence, no integration is required in Mach number control loop.

$$N_{com}\ = 251\sqrt{T}\ (1 - 0.454M)\ (\ M - M_{sp}) + N$$

The modeling of the gas flow system may require changes depending upon the performance of the boiler/evaporator, valve coefficients, line losses, and recovery compressor performance, resulting in the need for loop gain adjustments during commissioning. In mechanizing these integral control laws, appropriate mini-max clips are essential to prevent integral windup out of range in the controller software.

Nonlinear Modeling Equations

The differential equations representing the tunnel behavior form the basis for a nonlinear simulation of the tunnel dynamics for various control inputs covering the full operational envelope of the tunnel. A nonlinear simulation tool, capable of solving nonlinear differential equations, has been used for this work.[10] The differential equations, control laws, and identities have been solved for time variable using a Runge-Kutta-Fehlberg 4/5 order integration routine and the time trajectories for the tunnel dynamical responses have been obtained, over a period of 1500 seconds. The simplified numerical version of the equations used are:

$$W_g = 29803\,\frac{P}{T}\,(1 - 0.033\,M^2)$$

$$\gamma = 1.1415 - 0.000167\,T + P\,(0.02748 - 0.0000735\,T)$$

$$C_p = 221 + 35.01\,P + (1.49 - 0.09\,P)\,T$$

$$C_v = \frac{C_p}{\gamma} \qquad C_m = 5.5\,T - 0.008\,T^2 \qquad C_h = 385.4$$

$$t_m = \frac{2140}{T^{0.12}(P\,M)^{0.8}}$$

$$\dot{m}_t = 1800.4\,\frac{P\,M}{\sqrt{T}\left(1+\frac{(\gamma-1)}{2}M^2\right)^{\frac{(\gamma+1)}{2(\gamma-1)}}}$$

$$\text{power} = 15.95\,\frac{P\,M^3\sqrt{T}}{\left(1+\frac{(\gamma-1)}{2}M^2\right)^{\frac{(\gamma+1)}{2(\gamma-1)}}}$$

$$\Delta T = 0.150\,T\,M^2\left(\frac{\gamma-1}{\gamma}\right)$$

$$\text{wallheat} = 3\,\frac{(T - T_m)\,C_m}{t_m}$$

$$\frac{dP}{dt} = \frac{P}{W_g}(\dot{m}_s - \dot{m}_r - \dot{m}_{leak}) + \frac{P}{T}\frac{dT}{dt}$$

$$\frac{dT_m}{dt} = \frac{T - T_m}{t_m}$$

$$\frac{dT}{dt} = \frac{\text{power} - 0.001C_p(T + \frac{\Delta T}{2} - T_h - \delta h)\dot{m}_t - \text{wallheat}}{0.001W_g\, C_v}$$

$$\frac{dT_h}{dt} = \frac{0.001C_p\dot{m}_t(T + \frac{\Delta T}{2} - T_h - \delta h) - 1.28(T_h - \delta h - T_w)\, x_w}{42.9}$$

$$\delta h = \frac{1}{116 + 0.001C_p\dot{m}_t + 1.28\, x_w}\left\{0.001C_p\dot{m}_t\,(T + \frac{\Delta T}{2} - T_h) + 1.28\, x_w(T_h - T_w)\right\}$$

$$x_w = \frac{\dot{m}_t}{23}\left\{(T - T_{sp}) + 0.1\int(T - T_{sp})\right\} \text{ with minimax/windup clip } 0 < x_w < 100\ \%$$

$$x_s = 10\left\{(P_{sp} - P) + 0.03\int(P_{sp} - P)\, dt\right\} \text{ with minimax/windup clip } 0 < x_s < 100\%$$

$$\dot{m}_s = 0.2535\,\frac{P_{sf}}{\sqrt{T}}\,A_s \text{ where } A_s{=}0 \text{ for } 0{<}x_s{<}2 \text{ and } A_s = \left(\frac{x_s}{100}\right)^{1.7} \text{ for } 2 < x_s < 100\%$$

$$x_r = 10\left\{(P_{sp} - P) + 0.03\int(P_{sp} - P)\, dt\right\} \text{ with minimax/windup clip } 0 < x_r < 100\%$$

$$\dot{m}_r = 0.1811\,\frac{P}{\sqrt{T}}\,A_r \text{ where } A_r{=}0 \text{ for } 0{<}x_r{<}2 \text{ and } A_r = \left(\frac{x_r}{100}\right)^{1.7} \text{ for } 2 < x_r < 100\ \%$$

$$\dot{m}_{leak} = 0.02786\,\frac{P}{\sqrt{T}} \text{ for } P > 1.5 \text{ atm}$$

Simulation results

A number of simulation runs were performed and the control loops were tuned through a number of iterative runs to obtain good responses. The results of the dynamical simulation of the tunnel with the control system for three loops, in the form of time trajectories, are presented in figures 10a to 10k. Each figure shows six time-trajectories covering a period of about 1500 seconds. The tunnel total pressure P, temperature T, and Mach number M, are shown adjacent to their dominant and corresponding control inputs namely SF_6 gas valves strokes (inlet and recovery), water valve stroke, and fan speed.

Figure 10a shows the tunnel time response simulation for the initial conditions of Mach number M=0.8, total pressure P=3 atm, and all temperatures (heat exchanger, water, tunnel structure, and gas) at 303 K. The pressure set point is P_{sp}=6 atm and temperature set point is T_{sp}=319.4 K. The tunnel takes nearly 1100 seconds to build up pressure from 3 atm to 6 atm, consistent with the maximum mass inflow rate of 0.27 kg/s. The charging valve remains full open until the tunnel pressure reaches 6 atm. An oscillatory dynamic involving both charge and recovery valves hold the pressure to 6 atm. After reaching steady state pressure, the charge valve remains slightly open to accommodate for tunnel gas leaks. The tunnel gas temperature, exit water temperature, and average structural temperature are shown in the temperature plot. The tunnel gas temperature quickly increases from 303° K to 319.4° K and overshoots, but the water valve opens to maintain the gas temperature at the temperature set point. The exit water temperature remains about 8° K below the gas temperature at the start and grows to 17° K at full power. The tunnel walls take nearly 900 seconds to reach the gas temperature. The water flow control valve steadily opens as the tunnel pressure/power is increased. The valve is nearly fully open at P=6 atm, M=0.8, and T=319.4° K. Since fan speed and Mach number are held constant, no dynamics is evident. All the three loops are stable.

Figure 10b shows the simulation of the tunnel dynamics for a similar situation as in figure 10a except that the tunnel starting total pressure is P=5 atm and the set point is P_{sp}=4 atm. The pressure is reduced by the recovery system at mass flow rate of 0.137 kg/s. The tunnel takes nearly 800 seconds to decrease the pressure to 4 atm. An oscillatory dynamics settles the pressure to the final value. The temperature dynamics is similar to the previous case, except that the water valve trajectory is different. The exit water temperature is about 12°K lower than the gas temperature. The metal wall heat absorption keeps the water valve steady at about 35% open. This is due to reduced fan power at the lower final value of the pressure.

Figure 10c shows the tunnel state trajectories for initial conditions of M=0.30, P=1.9 atm, and all initial temperatures at 303°K. The pressure set point is P_{sp}=2 atm and temperature set point is T_{sp}=309.4°K. The pressure settles to final value within 50 seconds, both valves being active. Due to low fan power, the difference between the exit water temperature and the tunnel gas temperature is very low; both trajectories almost overlap each other. The temperature reaches 309.4° K in about 150 seconds and the water valve opens to allow small amounts of water flow. These trajectories demonstrate the control at low power conditions.

Figure 10d shows tunnel state trajectories at low fan power at a higher tunnel pressure than figure 10c. The simulation starts with a initial conditions of Mach number at 0.3, pressure of 6 atm, and all temperatures of 303° K. The control set points are 5.5 atm and 309.4° K. At this relatively low fan power, the tunnel takes nearly 100 seconds to reach the desired temperature. The difference between gas and heat exchanger temperature remains low and again the trajectories almost overlap each other. The tunnel pressure drops at the recovery system mass removal rate and settles after 400 seconds.

Figure 10e and 10f show simulations where the Mach number set point is programmed in an increasing direction at constant temperature of 319.4 K. This type of sweep is a typical Reynolds number/Mach number sweep performed during an aerodynamic test. The Mach number is swept from 0.4 to 0.8 in three steps with a dwell time of about 400 seconds. The dwell is intended for tunnel conditions to settle and for aerodynamic data acquisition after streamlining of the tunnel flexible walls. The Mach number is changed from 0.4 to 0.6 at 400 seconds and changed again from 0.6 to 0.8 at 900 seconds. In figure 10e, the pressure is kept constant at 3 atm throughout the test and the tunnel Reynolds numbers correspond to 9.8 million, 13.35 million, and 15.72 million (chord of 0.18 m) for M=0.4, 0.6, and 0.8 respectively. The gas temperature reaches the set point of 319.4° K in about 200 seconds. The exit water-gas temperature difference grows from a small value at M=0.4 to about 8° K at M=0.8. The tunnel structure takes about 1400 seconds to reach the gas temperature. The water valve is initially closed for about 200 seconds to allow the gas temperature to increase, and gradually reaches 20% open condition at M=0.8. Figure 10f shows a similar simulation where the operating pressure is 6 atm, and the corresponding Reynolds numbers are approximately 19.6 million, 26.7 million and 31.44 million (chord of 0.18 m) at M=0.4, 0.6 and 0.8 respectively. The water valve is fully open when the Mach number reaches 0.8. The exit water temperature drops by nearly 16° K at this power. The pressure and temperature trajectories are consistent with power effects.

Figures 10g and 10h shows similar trajectories for a descending Mach number sweep at two pressures of P=5 and 2 atm, for a constant temperature set point of 319.4° K. In this aerodynamic test the Reynolds numbers correspond to 16.3 million, 22.3 million, and 26.2 million (chord of 0.18 m) for M=0.4, 0.6, and 0.8 respectively. The tunnel process and controls demonstrate the time required for the tunnel to settle before data acquisition can start. Figure 10g demonstrates the trajectories for 5 atm total pressure where as the figure 10h shows a similar sweep for 2 atm total pressure.

Figure 10i shows an ascending Mach number sweep of M=0.4, 0.6, and 0.8. In the middle of this sweep the temperature set point has been changed from 315.4° to 319.4°K at a fixed pressure of 1.8 atm and a Mach number of 0.6. The Reynolds number changes with Mach number and with temperature, and the latter can be used for fine tuning the Reynolds number. The responses demonstrate the temperature control effectiveness of the closed loop control system using the water cooling system. The temperature settles within a short time, with a minimum overshoot.

Figure 10j shows a set of tunnel trajectories in which the Reynolds number has been changed using pressure at Mach numbers 0.5 and 0.8. The tunnel temperature is at 319.4° K. Reynolds number is varied from 11.5 million to 13.4 million at M=0.5, whereas at M=0.8 the Reynolds numbers varied from 15.3 million and 17.8 million (chord of 0.18 m). The aerodynamic data acquisition, including the wall adaptation, can be performed in this time period of about 1500 seconds. Though the valve movements appear to be large, the tunnel pressure is held within the band of ±0.05 atm initially, and within 0.005 atm after settling, as illustrated in figure 10k. The responses in figure 10k are duplicates of figure 10j with an enlarged vertical scale for pressure and gas valve positions. The pressure and gas valve area plots illustrate the effects of the nonlinear area-stroke relationship on the control of the tunnel.

These simulations demonstrate the typical characteristics of the water cooled SF_6 gas tunnel, and the adequacy of the control laws over the full envelope of the modified 0.3-m TCT operations. Generally, the tunnel states move slowly due to low rates of mass addition and removal and, hence, require relatively long settling times for pressure changes. The control laws are reasonably robust, but may require gain tuning during commissioning due to uncertainties in the gas flow and water flow modeling. These simulations confirm the closed loop control laws to be mounted on the controller.

Control Law Mechanization Issues

The control laws derived in this analysis are to be mechanized on the existing microprocessor-based cryogenic-mode controller hardware described in references 4 and 11. Since the option of running either the cryogenic mode or the SF_6 mode is to be provided, the following additions are proposed. The existing hard disk controller memory will be used to house two programs, one for control of the cryogenic mode, and a second new program for the SF_6 mode of operation. The second program is based on the analysis performed in this document. During the tunnel operation, the appropriate code is loaded to the Random Access Memory (RAM) and the Central Processing Unit (CPU) performs the control computations and functions through the real-time devices. The Table 3 lists the sensors and actuators for both modes of 0.3-m TCT operation.

Table 3

Input name	Sensor	Range	Volt/amps	
E(1)	PP (P)	0-88 psia	0-5 VDC	
E(2)	PS (P_s)	0-88 psia	0-5 VDC	
E(3)	TT (T)	78-342 K	0-5 VDC	
E(4)	TMWL(T_m)	78-342 K	0-5 VDC	Existing sensors for cryogenic tunnel and all except PLQ will be required for SF_6 gas operation also
E(5)	FRPM (N)	0-6400 rpm	0-5 VDC	
E(6)	PLQ	0-300 psig	1-5 VDC	
E(7)	DLP	0-5 psid	0-5 VDC	
E(8)	-	-	-	
E(9)	PSF (P_{sf})	0-300 psia	0-5 VDC	
E(10)	RSF (P_b)	0-100 psia	0-5 VDC	
E(11)	TWI (T_w)	273-330 K	0-5 VDC	New sensors for SF_6 gas tunnel (New ADC Hardware)
E(12)	TWO (T_h)	273-330 K	0-5 VDC	
E(13)	SFCN (κ)	50-100%	0-5 VDC	
E(14)	PST(P_{st})	0-500 psig	0-5 VDC	
E(15)	-	-	-	
E(16)	-	-	-	
Output name	Actuator	Range	drive	
DAC(1)	ALQ	0-100%	4-20 ma	
DAC(2)	ALQ	0-100%	4-20 ma	
DAC(3)	ALN	0-100%	0-5 VDC	
DAC(4)	AGV1	0-100%	1-5 VDC	Existing actuator drives for cryogenic tunnel. Only SNRPM/ IQ will be used in SF_6 gas operation (SNRPM = 500-2500 rpm for SF_6)
DAC(5)	AGV2	0-100%	1-5 VDC	
DAC(6)	SNRPM	0-6400	0-5 VDC	
DAC(7)	IQ	Fan ref	5 VDC	
DAC(8)	-	-	-	
DAC(9)	AISF	0-100%	4-20 ma	
DAC(10)	AOSF	0-100%	4-20 ma	New actuator drives for the SF_6 mode of operation (New DAC hardware)
DAC(11)	AWV	0-100%	4-20 ma	
DAC(12)	-	-	-	

The Table 3 also lists existing and proposed software variable names. From the seven cryogenic mode tunnel transducers, six will be required and used in the SF_6 mode. In addition a new set of six sensors will be required for the SF_6 mode. The cryogenic mode generates seven commands to drive the actuators for controlling the tunnel. Only two of these seven, corresponding to fan speed control, will be necessary for the SF_6 mode. The other five drives will be set to zero during the SF_6 mode of operation. In addition, three new actuator drives for the SF_6 inlet valve, recovery system valve, and the water valve will be needed. All the new valves will be 4-20 milliamperes coil actuated flapper-nozzle driven, diaphragm operated, pneumatic valves. When reverting to the cryogenic mode of operation, the cryogenic mode software will be modified to signal zero currents to the SF_6 mode actuators. In each mode a sensor signal check module is used for emergency shutdown. The unused sensor signal check will be bypassed.

At the controller hardware level, two more real time devices will be necessary for the microcomputer. First is an analog to digital converter for the six new sensor channels with a 16 bit (1 in 65536) resolution requirement, so as to be compatible with the rest of the cryogenic mode controller. Second is a digital to analog converter for three new actuator channels of 12 bit (1 in 4096) resolution providing 4-20 milliamperes range signals to drive the SF_6 valves and water valves.

The structure of the SF_6 mode control software will be similar to the cryogenic mode software. The software will consist of a screen-format one-pass code, analog-to-digital conversion module, module for control laws for the three loops, key-board read module servicing one command per cycle, actuator drive, digital-to-analog conversion module, screen update module, and a sensor signal range based emergency module, all working in an endless loop. The compiled-executable code, after extensive testing for numerical robustness, will be mounted on the microcomputer controlling the 0.3-m TCT.

This code is expected to take about 100 milliseconds to execute a cycle, as in the case of the existing cryogenic mode software. A view of the proposed controller display layout is shown in figure 11. The tunnel will have provision for Pressure or Reynolds number control, Mach number control, and Temperature control. Using the information from the SF_6 concentration κ sensor, the Reynolds number estimation will be corrected for dilution of the SF_6 gas with air. A system shutdown will be necessary for changing the gas modes on the controller in order to invoke the proper software for the controller.

Conclusions

A study of the various performance and tunnel control issues related to the proposed modification of 0.3-m TCT to operate with sulfur hexaflouride (SF_6) gas are presented in this document. Utilizing the thermophysical properties of SF_6 gas and the modified tunnel geometry, a thermodynamic lumped mathematical model of the tunnel process has evolved. The various tunnel performance parameters like mass flow, circuit time, fan power, fan speed, and flow Reynolds number boundary have been estimated. The 0.3-m TCT modified for SF_6 operation will be capable of providing about 30 million Reynolds number per 0.18 m chord up to about Mach number of 0.8 at total pressure of 6 atm. The fan speed/heat exchanger limits on the Reynolds number envelope have been analyzed.

Control laws for closed loop control of the SF_6 tunnel states have been generated to provide control accuracy of ± 0.07 psi for pressure, ± 0.3°K for temperature, and ± 0.0015 for Mach number. The nonlinear simulation of the tunnel closed-loop control responses confirm the adequacy of the control laws to provide the desired accuracy of control. The simulation has covered the full envelope of the tunnel operation. The simulation shows that changes in tunnel pressure tend to be slow due to the limited SF_6 mass flow rates. The control laws for the SF_6 mode and the controller electronic hardware design aspects have been analyzed. Provisions exist for fine tuning the control laws to account for any variation in system stability, control, and responses that may be encountered during the commissioning phase of the tunnel in 1993. Such variations are likely due to uncertainties in modeling the tunnel process.

Acknowledgments

This work has been performed under NASA contract number NAS1-18585, Task-77 with John B. Anders, Jr as the task monitor. The authors wish to also acknowledge technical support in this work from Charles S. Ladson and Blair B. Gloss of the High Reynolds Number Aerodynamics Branch.

References

1. Goodyer, M. J. and Kilgore, R. A.; High Reynolds Number Cryogenic Wind Tunnel, AIAA Journal, Volume 11, No. 5, May 1973, pp 613-619.

2. Gloss, B. B.; Initial Research Program for the National Transonic Facility, AIAA Paper 84-0585, AIAA 13th Aerodynamic Testing Conference San Diego, California 1984.

3. Balakrishna, S.; Synthesis of a Control Model for a Liquid Nitrogen Cooled, Closed Circuit, Cryogenic Nitrogen Wind Tunnel and its Validation, NASA CR 162508, February 1980.

4. Balakrishna, S. and Kilgore, W. A.; Microcomputer based Controller for the Langley 0.3-Meter Transonic Cryogenic Tunnel, NASA CR 181808, March 1989.

5. Jenkins, R.; Program to calculate the Isentropic Flow Properties of Sulfur Hexaflouride, NASA Technical Memorandum 4358 , August 1992.

6. Brown, J. A.; Encyclopedia of Chemical Technology, 2nd Edition, Volume 9, pp 664-671, John Wiley 1966.

7. Pope, A.; Wind Tunnel Testing, John Wiley Publications, 1954.

8. Critical Design Review Document, NASA LaRC 1/3 M-Transonic Cryogenic Tunnel Modification Study to Use Heavy Gas Test Media, Sverdrup Technology, Inc, April 1992.

9. Lawing, P. L. and Johnson, C. B.; Summary of Test Techniques in the NASA Langley 0.3-m Transonic Cryogenic Tunnel, AIAA paper 86-0745 CP, AIAA 14th Aerodynamic Testing Conference, West Palm Beach, March 1986.

10. Elmquist, H.; Astrom, K. J.; Sconthal, T.; and Wittenmark, B.; SIMNON - Users guide, SSPA Systems, Sweden, January 1990.

11. Kilgore, W. A.; and Balakrishna, S.: The NASA Langley Research Center 0.3 Meter Transonic Cryogenic Tunnel Microcomputer Controller Source Code, NASA CR 189556, December 1991.

Appendix

Performance of the 0.3-m TCT with the inclusion of the new heat exchanger in Cryogenic nitrogen mode and the new Air mode

The 0.3-m TCT is being modified to operate with both cryogenic nitrogen and ambient temperature sulfur hexaflouride (SF_6) test gases. To operate with SF_6 gas, the tunnel will be fitted with a heat exchanger in the tunnel circuit. Hence, the cryogenic mode performance will change unless the heat exchanger is removed every time the tunnel reverts to the cryogenic mode. The addition of a heat exchanger also provides the possibility of a new air mode of operation for. The tunnel will require a new dry-air supply for air mode operation. This appendix presents the estimates of changes in the performance limits for the cryogenic mode, and the performance with the air mode of operation with heat exchanger in place.

With the introduction of the new heat exchanger in the tunnel circuit, the circuit loss pattern is now somewhat different. The following basic equations provide the power, speed, and Reynolds number identities for the new cryogenic tunnel circuit, and the identities utilize the thermophysical properties of nitrogen gas.

$$\text{Power} = \dot{m}_t\, C_p\, \Delta T = 338.9\, \frac{P}{T} \sqrt{\frac{8314\, \gamma\, T}{\text{mole}}}\; C_p\, b\, \frac{\gamma\text{-}1}{\gamma}\, A_t\, \frac{M^3}{\left(1+\frac{\gamma-1}{2} M^2\right)^{\frac{(\gamma+1)}{2(\gamma-1)}}}\ \text{kw}$$

$$\text{Fan speed} = N = 509 \sqrt{T}\, M\, (1 - 0.3M)\ \ \text{rpm}$$

$$\text{Reynolds number} = R_e = 63714\, \frac{P\ M\ \bar{c}}{T^{1.4}\, (1+0.2M^2)^{2.1}}\ \ \text{million } /\bar{c}$$

The tunnel circuit loss changes with tunnel Reynolds number. With nitrogen test gas, the modified tunnel circuit loss factor varies with operating temperature and can be estimated as:

$$r = 1.001 + 0.8765\, M^2\, R_{ft}^{\ -0.096} \ \simeq\ 1 + 0.160\, M^2$$

The envelope of tunnel operations in the Cryogenic mode have been estimated using values of C_p=1.04, γ=1.41, A_t=0.109, b=0.160 at 100° K, 0.172 at 200°K and 0.188 at

300° K, mole=28.2, and $\overline{c}$=0.18 m. This assumes that the heat exchanger has been dried and that liquid nitrogen is sprayed into the tunnel to control the nitrogen mass and temperature. Figures A1, A2, and A3 provide the tunnel Power-Mach number plot for three typical temperatures of 100°K, 200°K, and 300°K. The plots also show the 6 atm case with no heat exchanger in the tunnel circuit to provide an estimate of the deterioration in peak performance due to extra circuit losses from the heat exchanger. The plots also shows the speed band, 3550-3650 rpm, which is a singularity for the drive system. The maximum speed locus of 5600 rpm is also shown in figure A3. Figures A4, A5, and A6 show the Reynolds number-Mach number envelope of the tunnel at 100°K, 200°K, and 319.4°K.

In the air mode of operation, the tunnel air mass is controlled through a dry air supply. The tunnel temperature is controlled using control of the water flow rate through the heat exchanger thereby removing the heat from tunnel flow. The estimation of power, speed, and Reynolds number are the same as the cryogenic nitrogen case since thermophysical properties of air are essentially the same as nitrogen, for purposes of this study. However, the power usable in the tunnel circuit is limited by the amount of heat that can be removed by the heat exchanger. The heat exchanger is designed to remove 550 kw of heat at 5 atm, M=0.8 and T=319.4°K with an inlet water temperature of 303°K. Without performing heat exchange calculations at off-design conditions, an operational envelope for the tunnel is shown in figure A6. This has been estimated with a circuit loss factor of 0.189. Figure A6 shows the loci of power equilibria at 550, 500, 400 and 300 kw with the tunnel air temperature at 319.4°K. The capacity of the heat exchanger to remove heat changes with the inlet water temperature which may vary from 289 to 306°K. With the heat exchanger working at its designed capacity of 550 kw, the tunnel can provide Reynolds number of about 10 million/0.18 m chord at about M=0.5 and P=6 atm. It drops to 4 million/0.18 m chord at M=0.81 and 2 atm. However, since the 0.3-m TCT flexible walls can be moved to an effectively lower A_t(<0.109 m^2), slightly higher Reynolds number performance can be obtained.

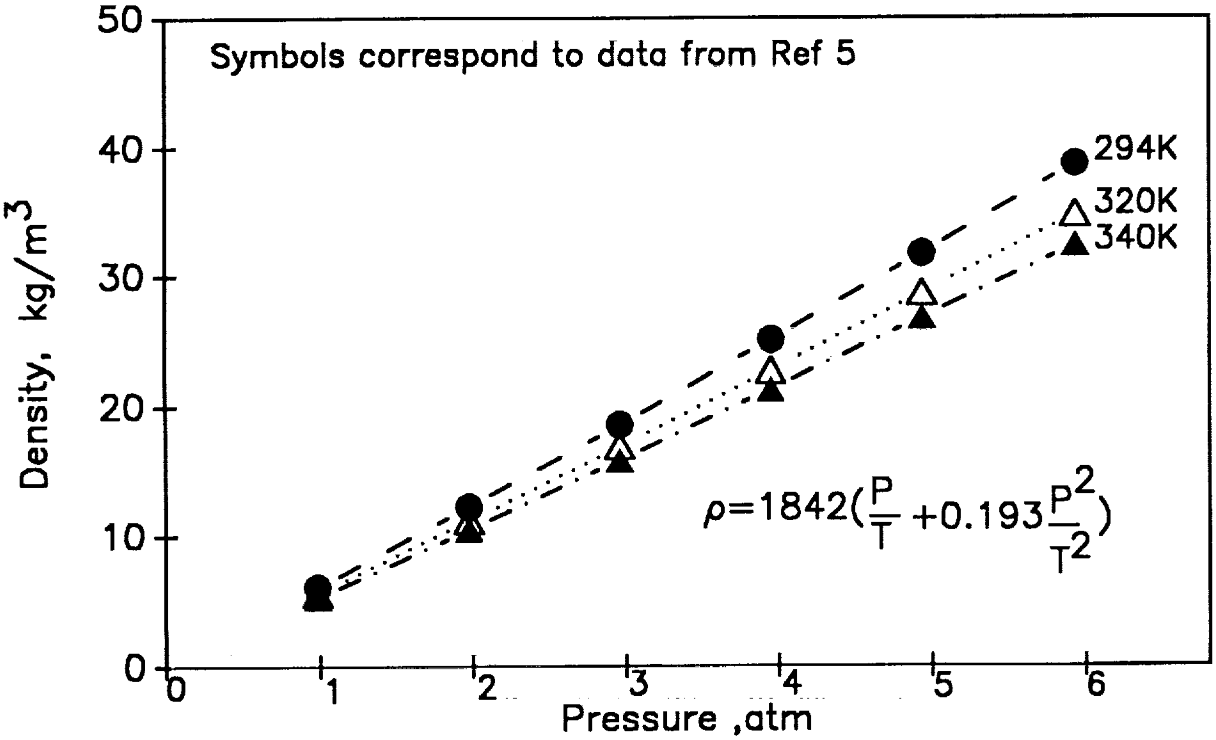

Figure 1: Density of Sulfur Hexaflouride

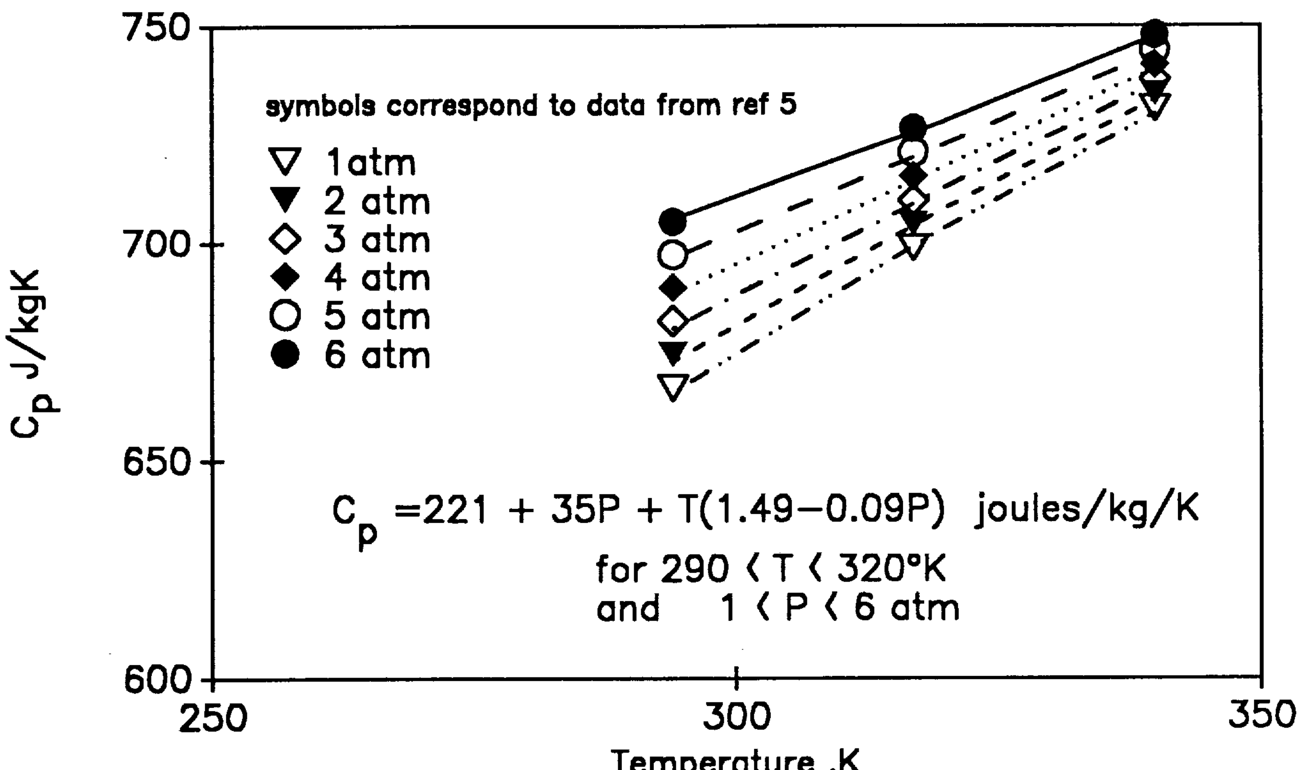

Figure 2 : Specific Heat C_p for Sulfur Hexaflouride

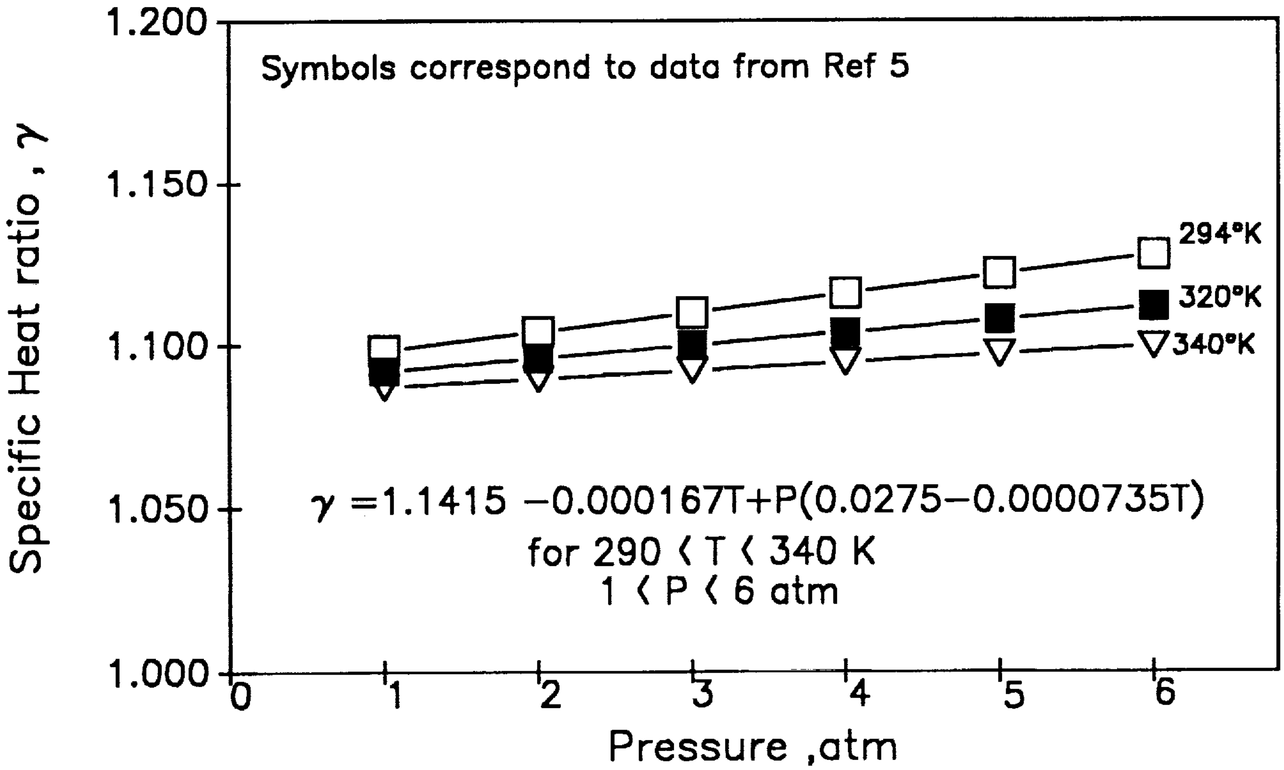

Figure 3: Specific heat ratio for Sulfur hexaflouride

Figure 4: Schematic of 0.3-m TCT modified for Sulfur Hexafloride Gas Medium

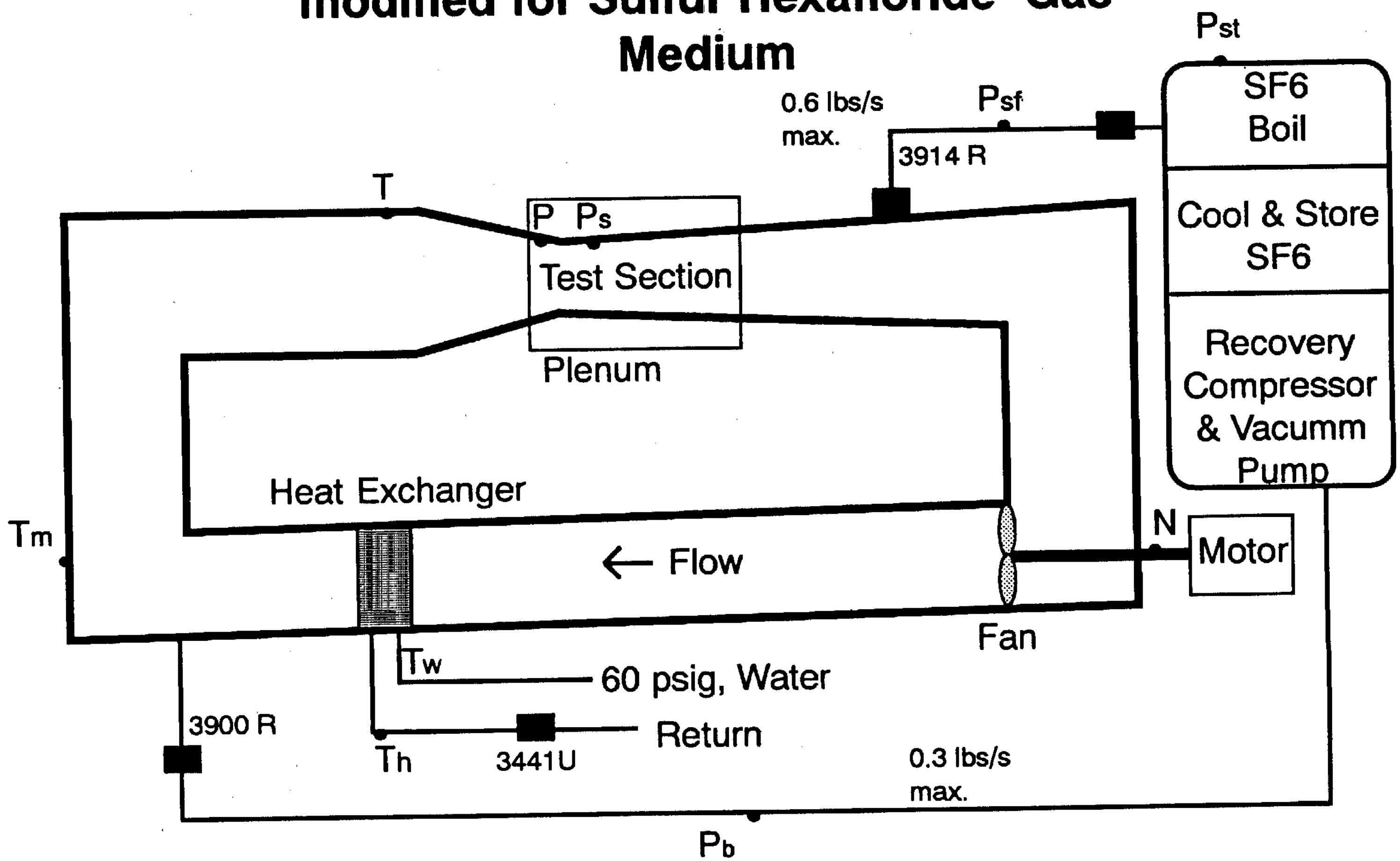

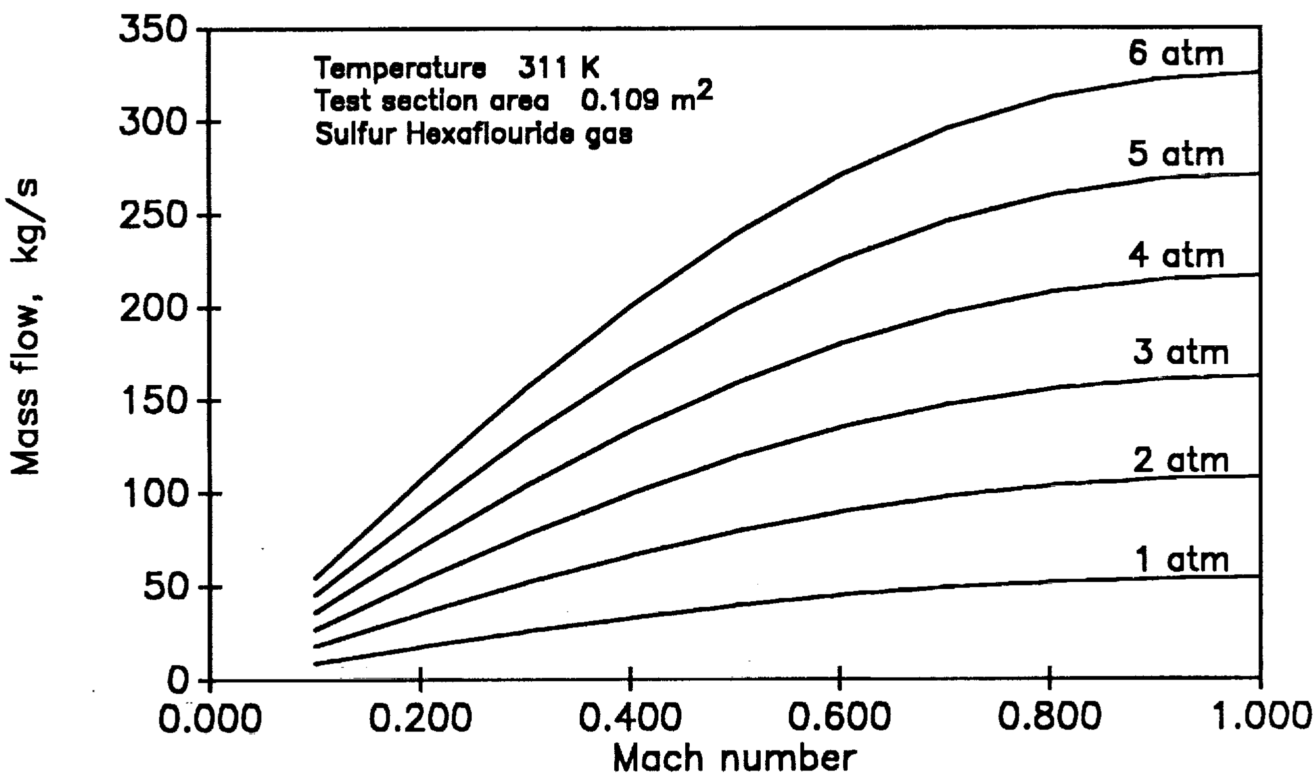

Figure 5: Tunnel Test Section Mass Flow

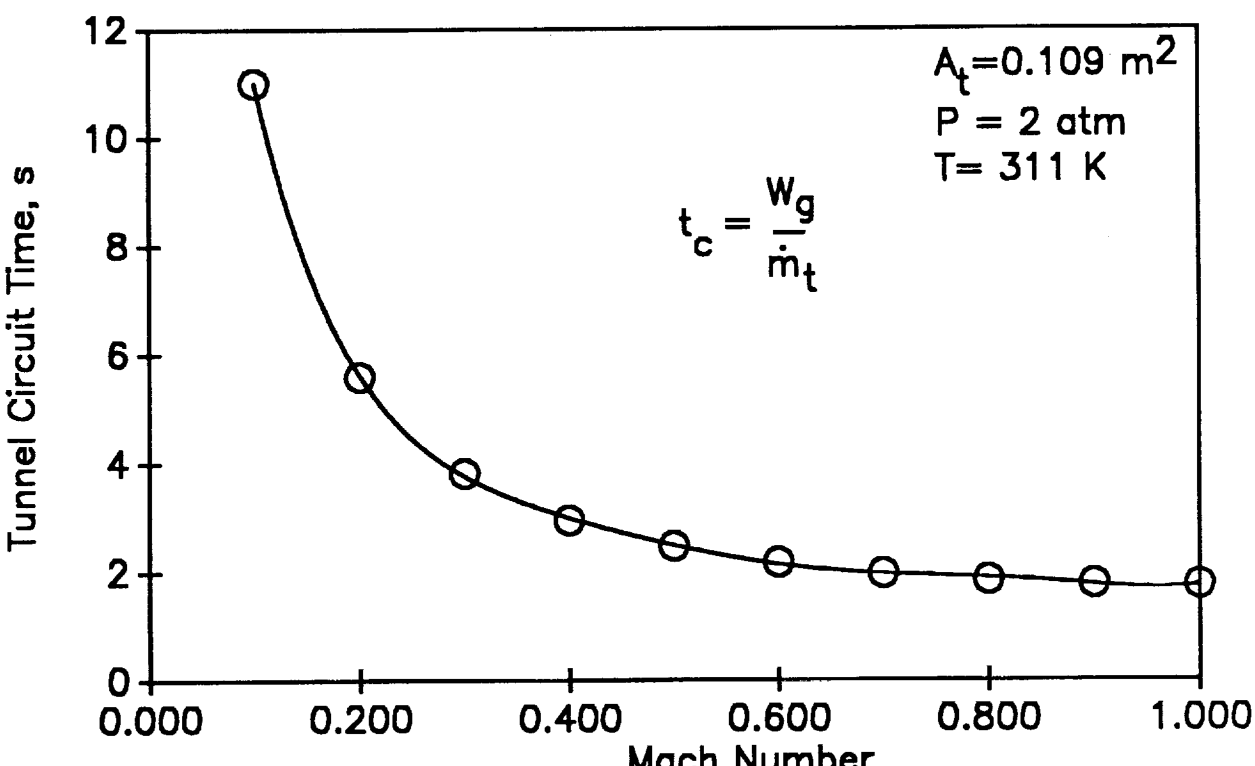

Figure 6: Tunnel circuit time

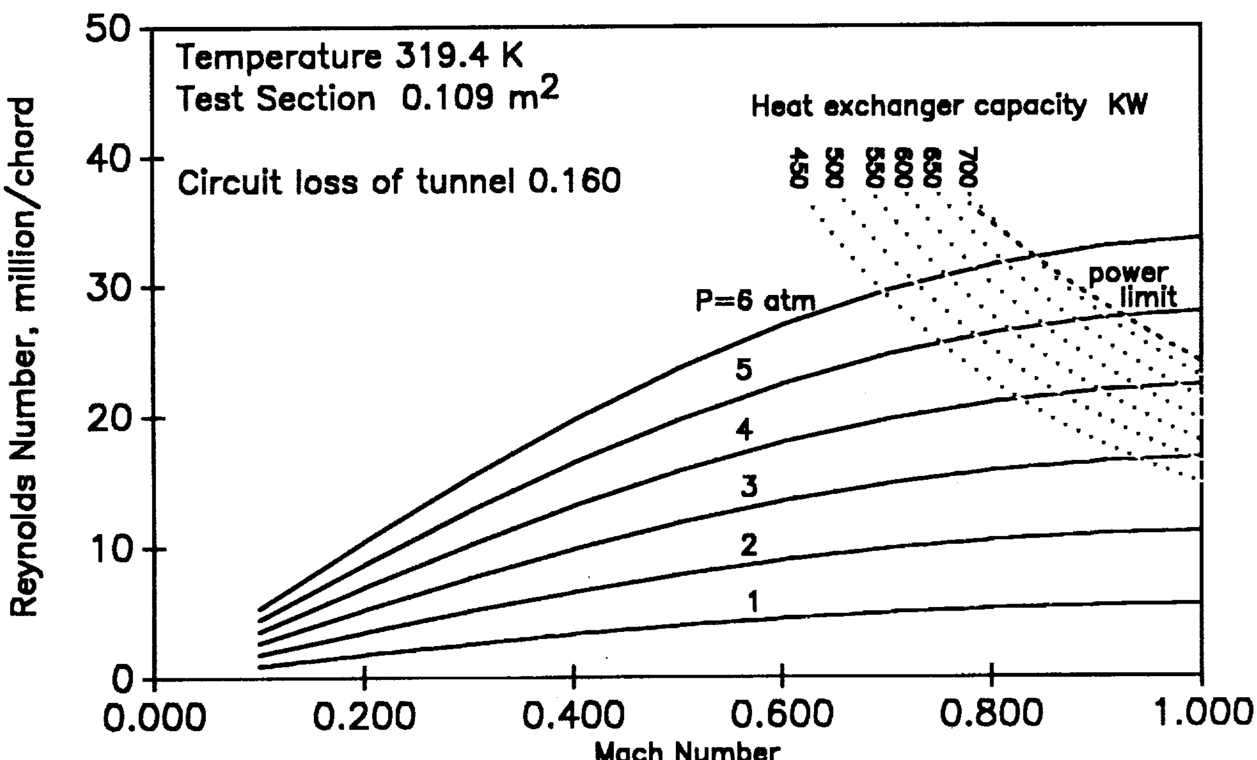

Figure 7:Reynolds Number Operating Envelope

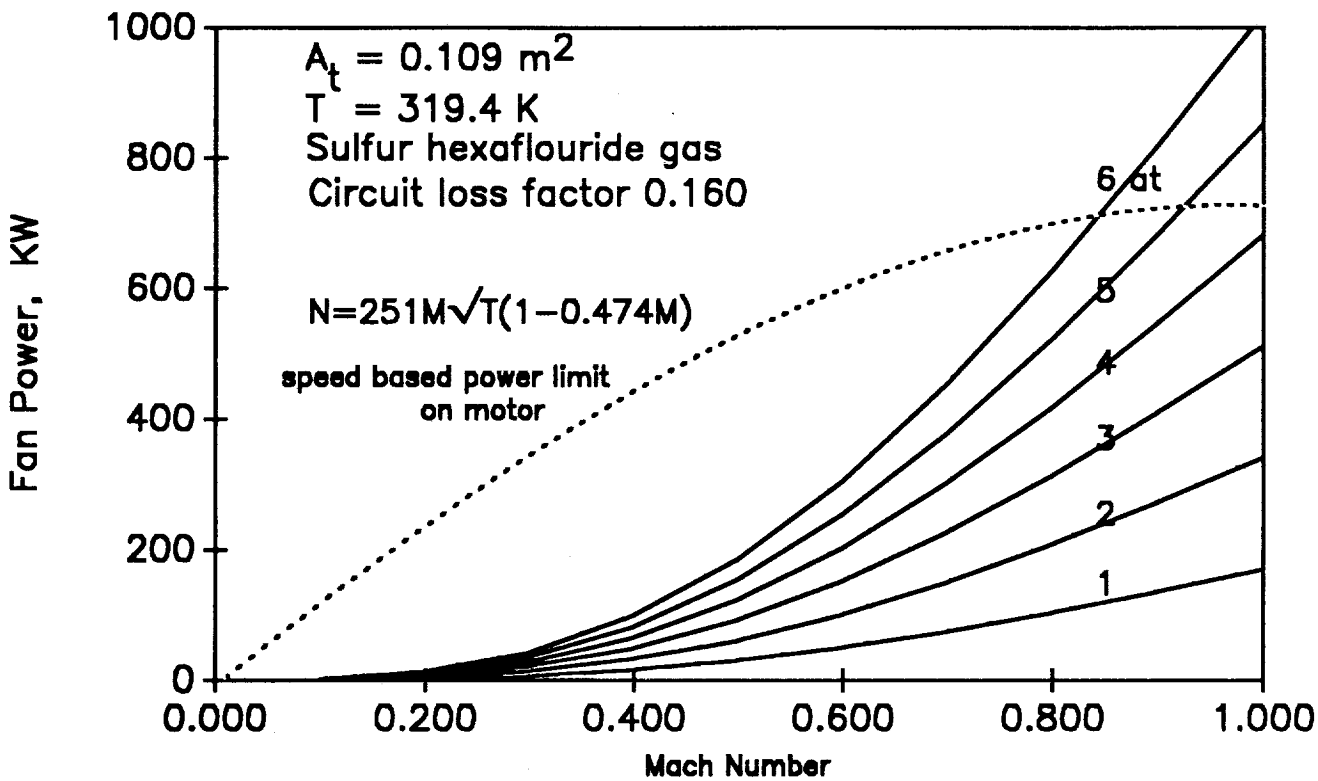

Figure 8: Fan power Requirements

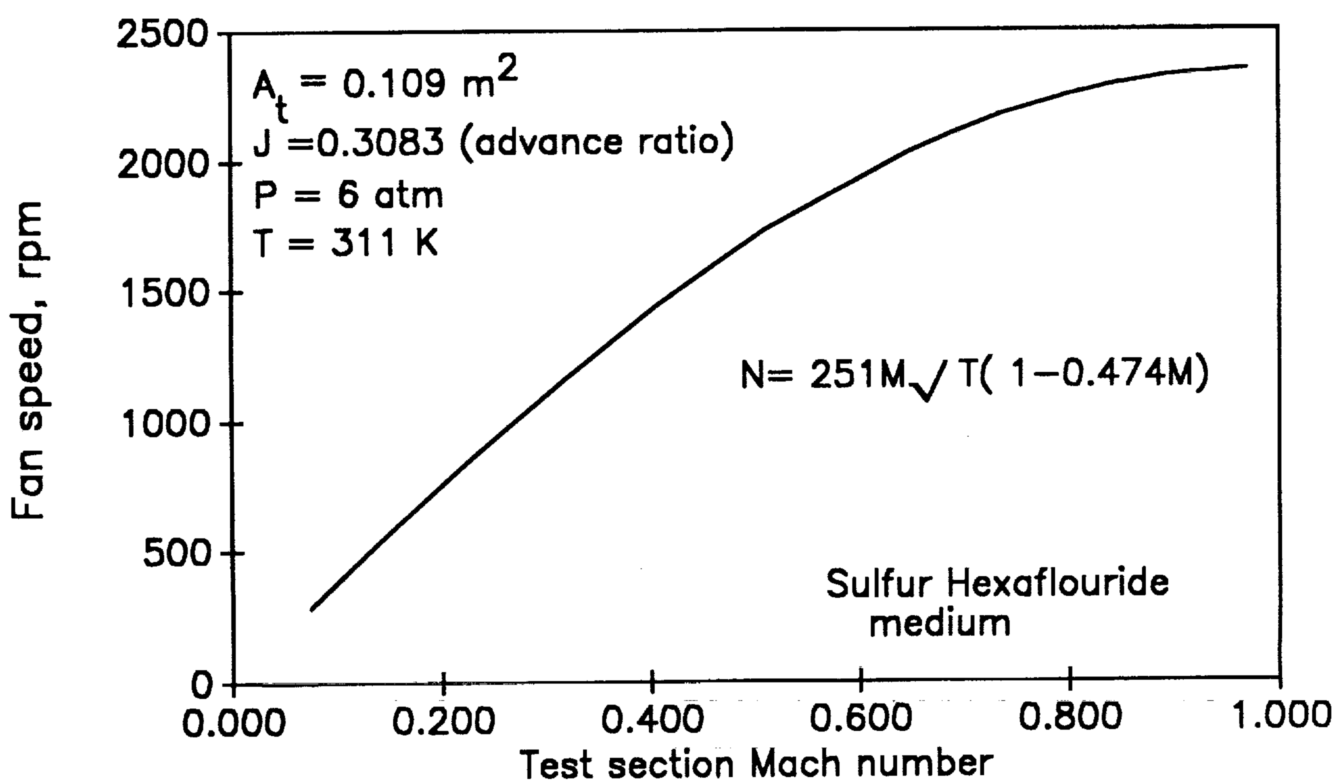

Figure 9 : Fan speed Requirements

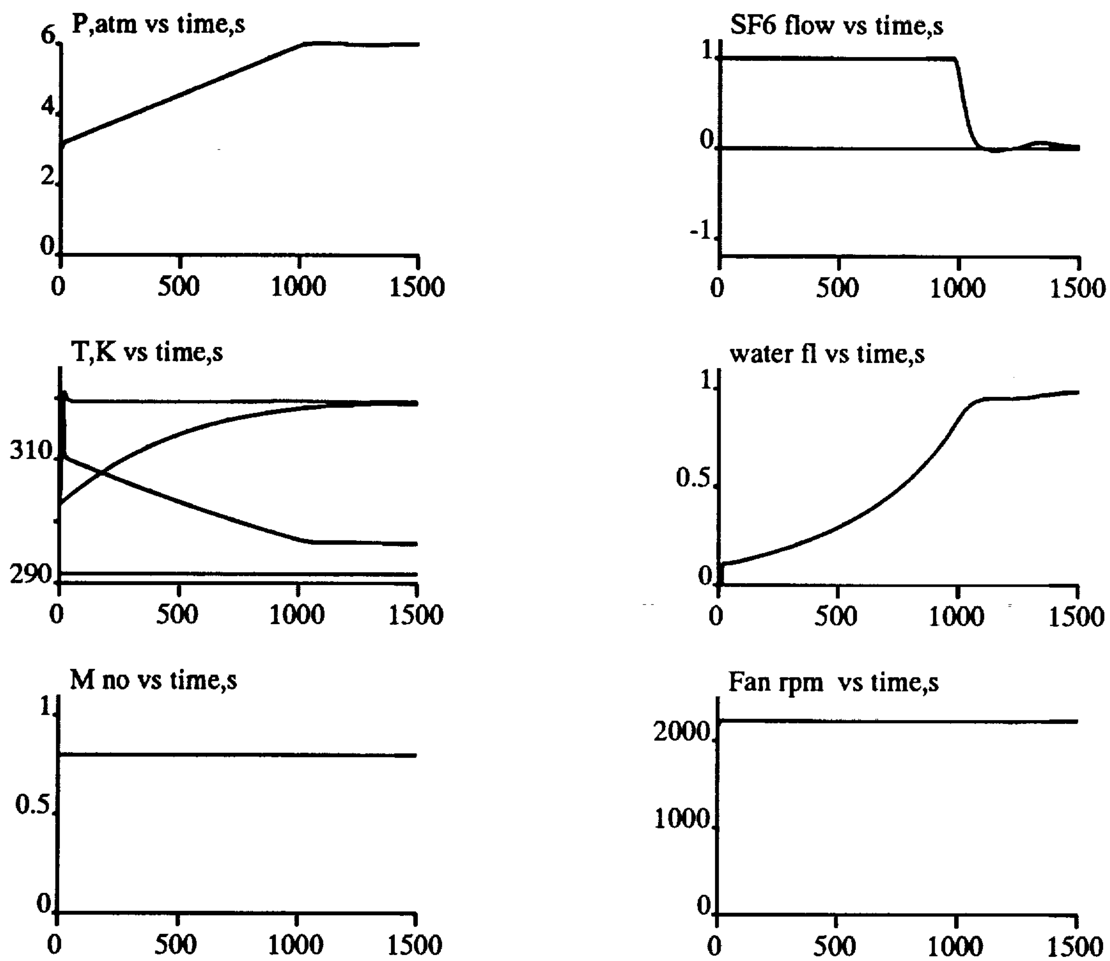

Figure 10a: Simulation of Tunnel Responses

Initial conditions : P=3 atm, T=303 K, M=0.8
Set points : P=6 atm, T=319.4 K
M= 0.8
Temperature plots show in descending order Gas,Metal wall (exponential)
Exit water & Sump water (291.5K) temperatures
Gas valves correspond to + for charging & – for recovery
Valves correspond to 0 for close and 1 for full open

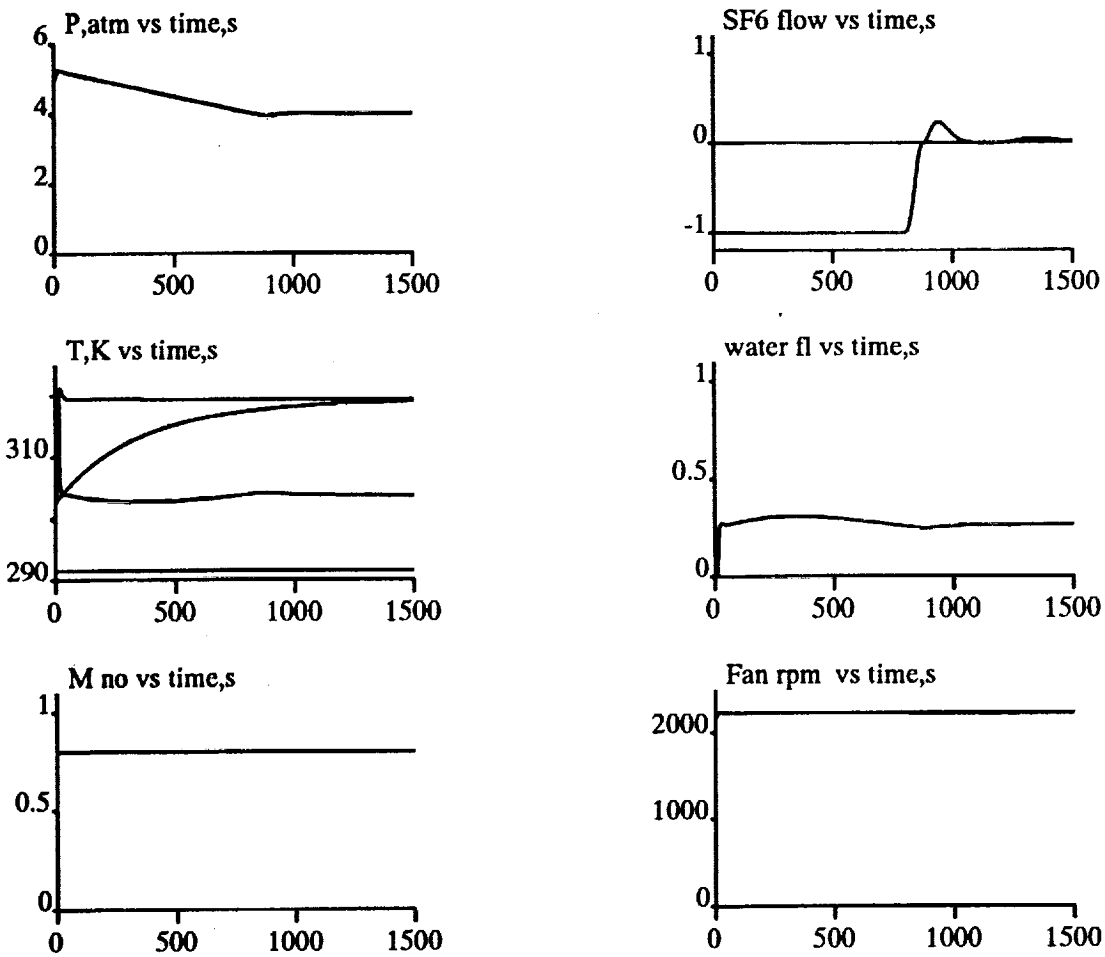

Figure 10b: Simulation of Tunnel Responses

Initial conditions : P=5 atm, T=303 K, M=0.8
Set points : P=4 atm, T=319.4 K
M= 0.8
Temperature plots show in descending order Gas,Metal wall (exponential)
Exit water & Sump water (291.5K) temperatures
Gas valves correspond to + for charging & − for recovery
Valves correspond to 0 for close and 1 for full open

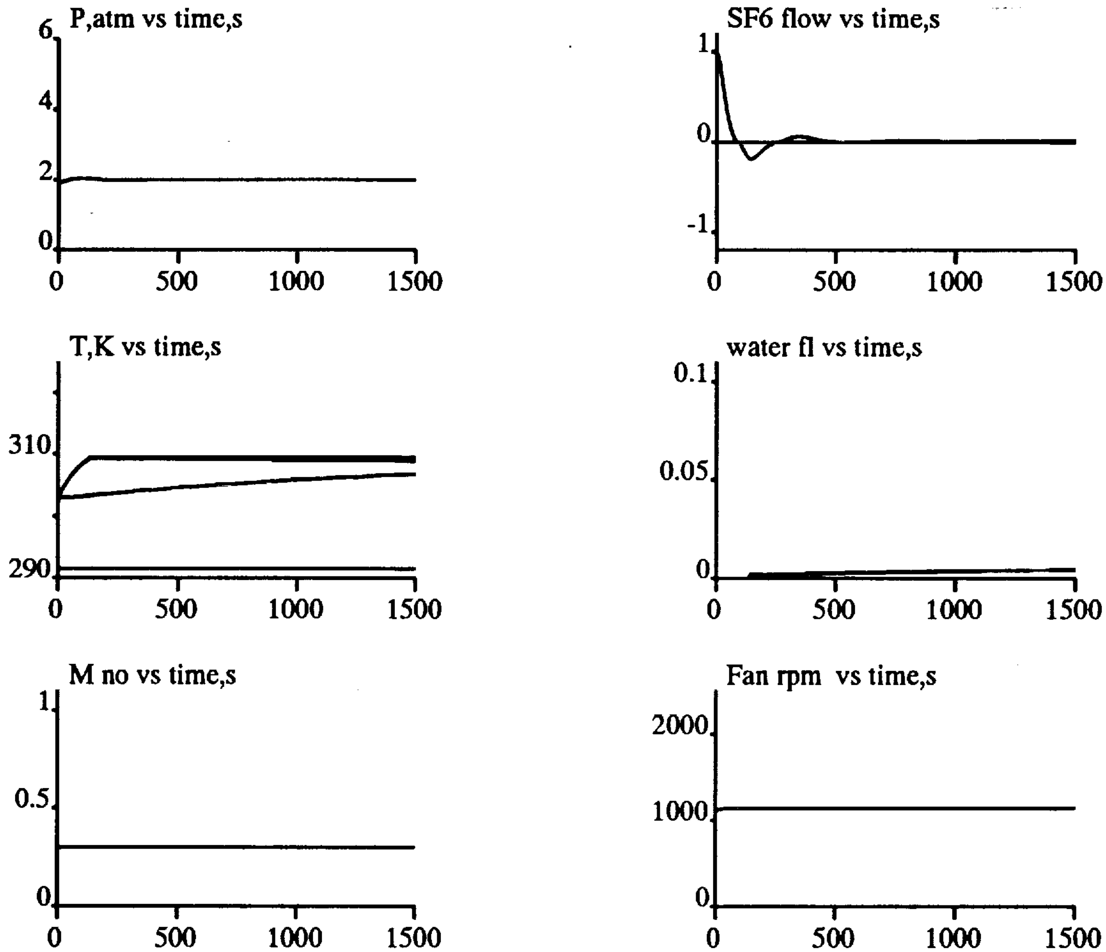

Figure 10c: Simulation of Tunnel Responses

Initial conditions : P=1.9 atm, T=303 K, M=0.3
Set points : P=2 atm, T=309.4 K
M= 0.3
Temperature plots show in descending order Gas,Exit water(overlapping)
Metal wall(exponential) & Sump water (291.5K) temperatures
Gas valves correspond to + for charging & – for recovery
Valves correspond to 0 for close and 1 for full open

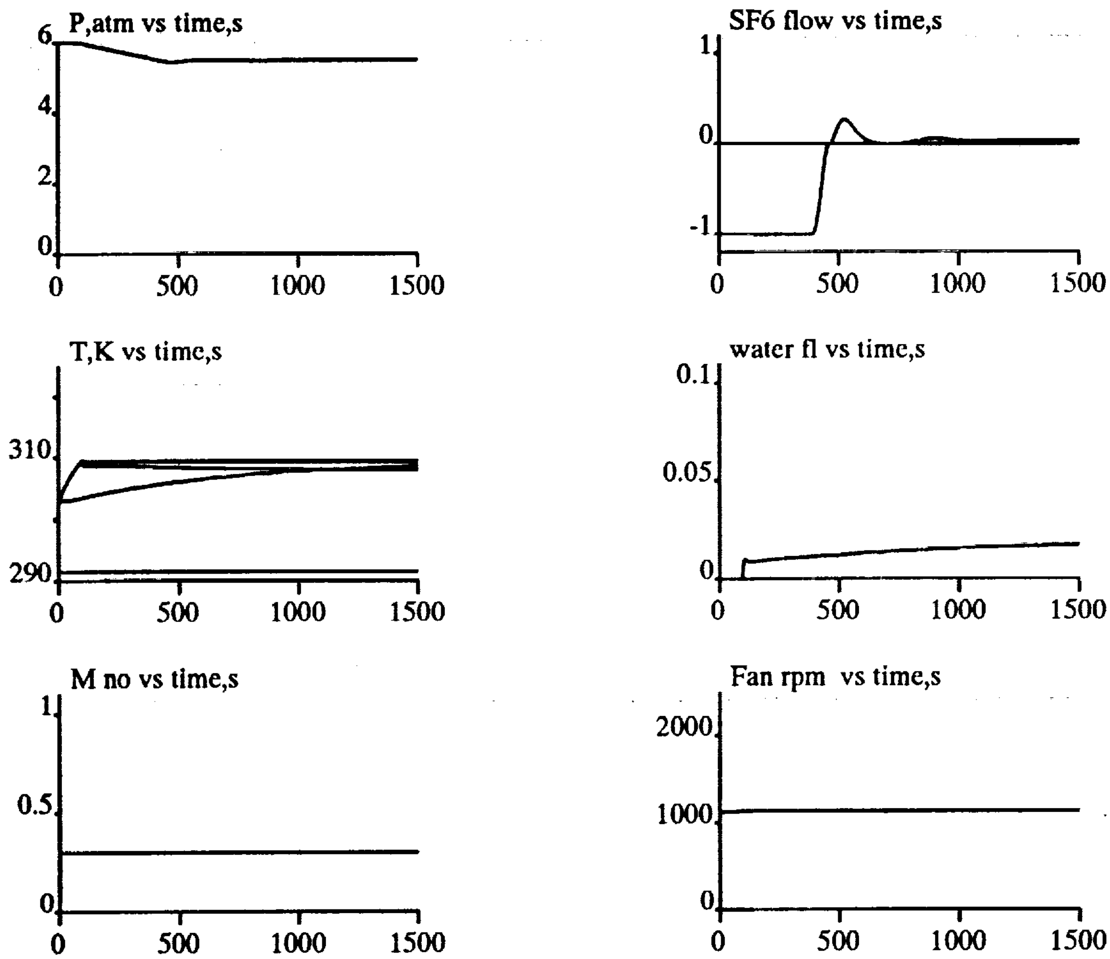

Figure 10d: Simulation of Tunnel Responses

Initial conditions : P=6 atm, T=303 K, M=0.3
Set points : P=5.5 atm, T=309.4 K
M= 0.3
Temperature plots show in descending order Gas,Exit water(overlapping)
Metal wall(exponential) & Sump water (291.5K) temperatures
Gas valves correspond to + for charging & − for recovery
Valves correspond to 0 for close and 1 for full open

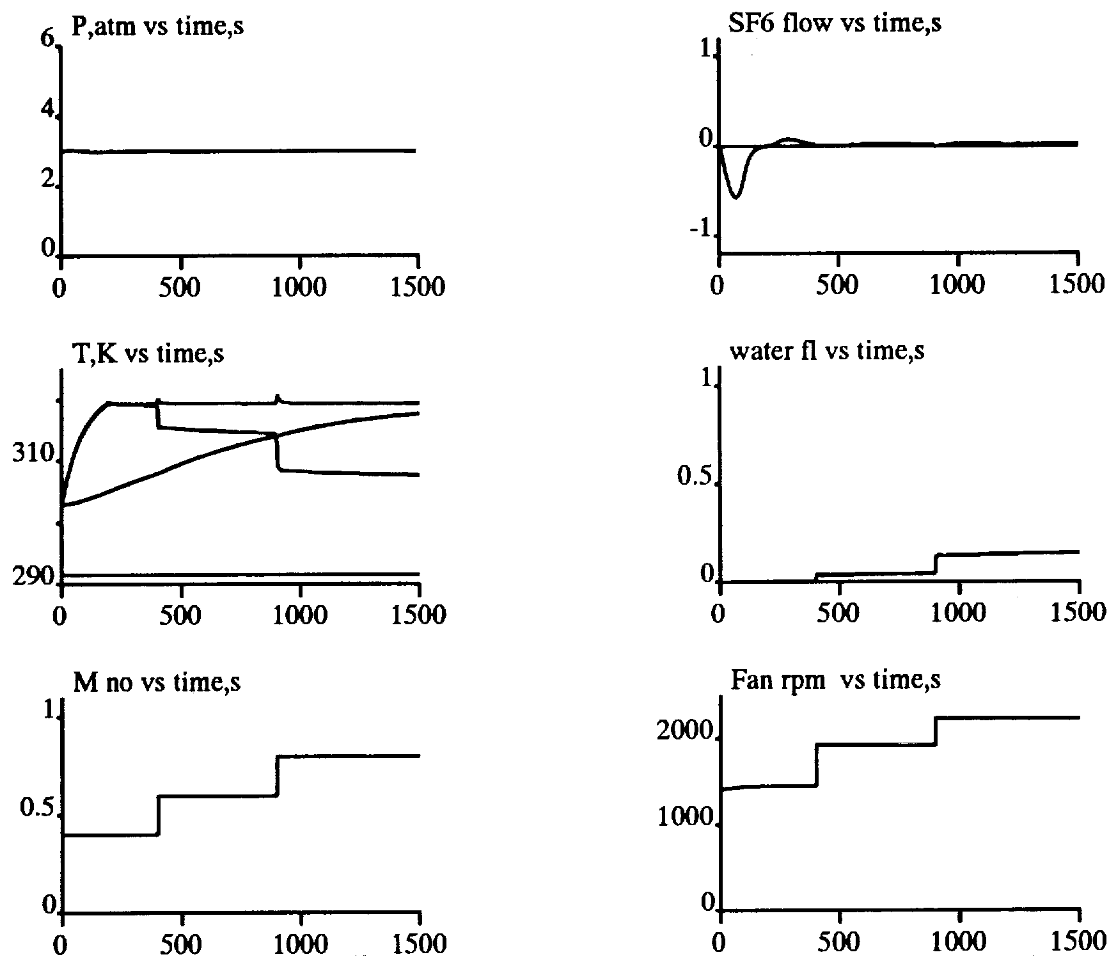

Figure 10e: Simulation of Tunnel Responses

Initial conditions : P=3 atm, T=303 K, M=0.4
Set points : P=3 atm, T=319.4 K
M= 0.6 at 400 s and 0.8 at 900 s
Temperature plots show in descending order Gas, Metal wall(exponential)
Exit water & Sump water (291.5K) temperatures
Gas valves correspond to + for charging & − for recovery
Valves correspond to 0 for close and 1 for full open

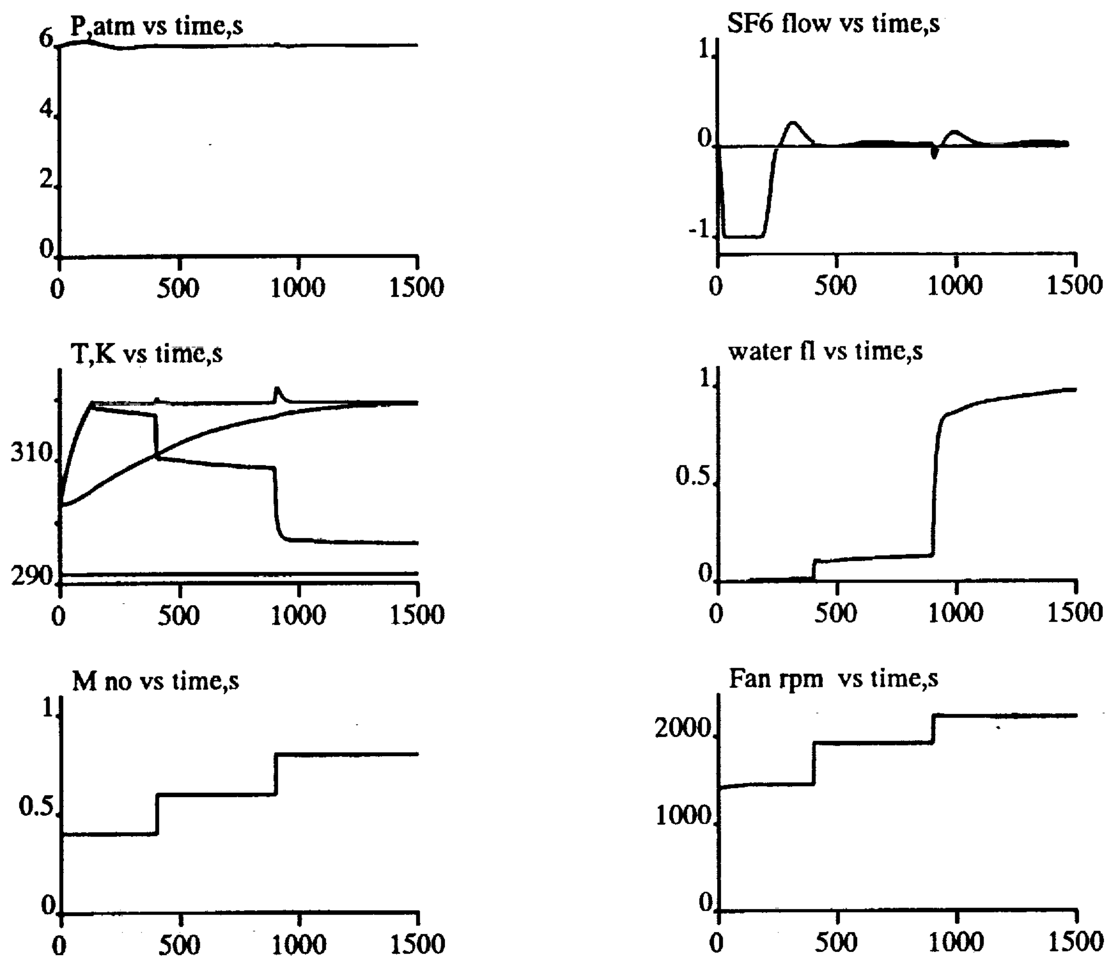

Figure 10f: Simulation of Tunnel Responses

Initial conditions : P=6 atm, T=303 K, M=0.4
Set points : P=6 atm, T=319.4 K
M= 0.6 at 400 s and 0.8 at 900 s
Temperature plots show in descending order Gas, Metal wall(exponential)
Exit water & Sump water (291.5K) temperatures
Gas valves correspond to + for charging & – for recovery
Valves correspond to 0 for close and 1 for full open

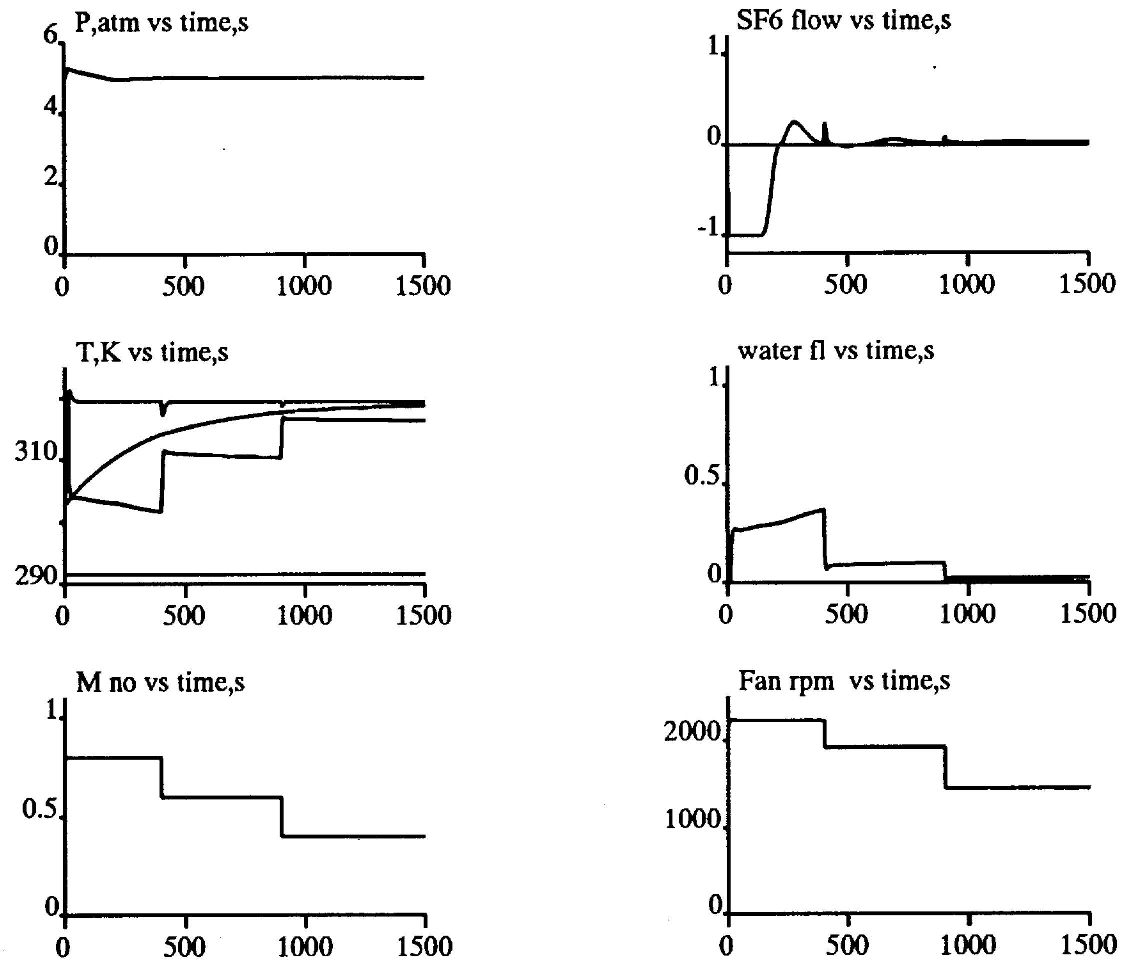

Figure 10g: Simulation of Tunnel Responses

Initial conditions : P=5 atm, T=303 K, M=0.8
Set points : P=5 atm, T=319.4 K
M= 0.6 at 400 s and 0.4 at 900 s
Temperature plots show in descending order Gas, Metal wall(exponential)
Exit water & Sump water (291.5K) temperatures
Gas valves correspond to + for charging & − for recovery
Valves correspond to 0 for close and 1 for full open

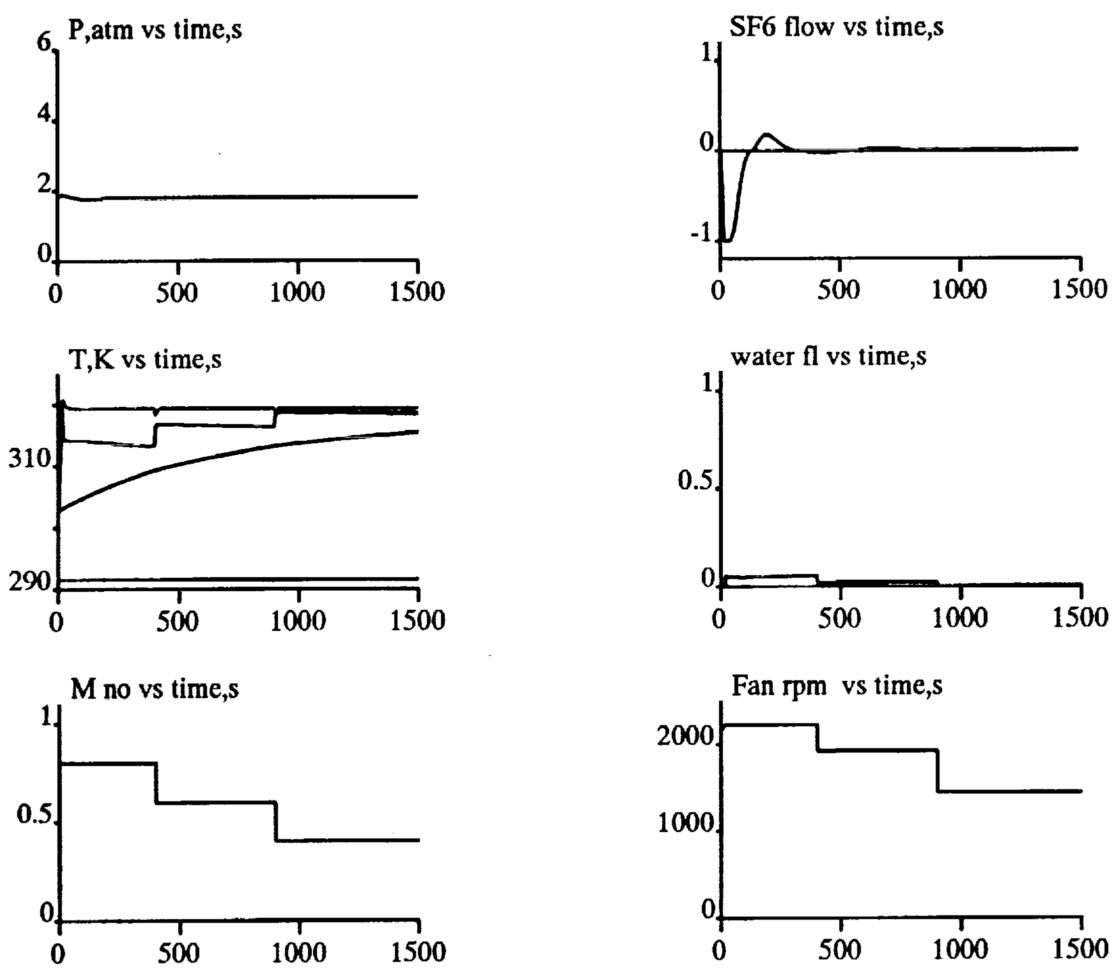

Figure 10h: Simulation of Tunnel Responses

Initial conditions : P=1.8 atm, T=303 K, M=0.8
Set points : P=1.8 atm, T=319.4 K
M= 0.6 at 400 s and 0.4 at 900 s
Temperature plots show in descending order Gas, Metal wall(exponential)
Exit water & Sump water (291.5K) temperatures
Gas valves correspond to + for charging & − for recovery
Valves correspond to 0 for close and 1 for full open

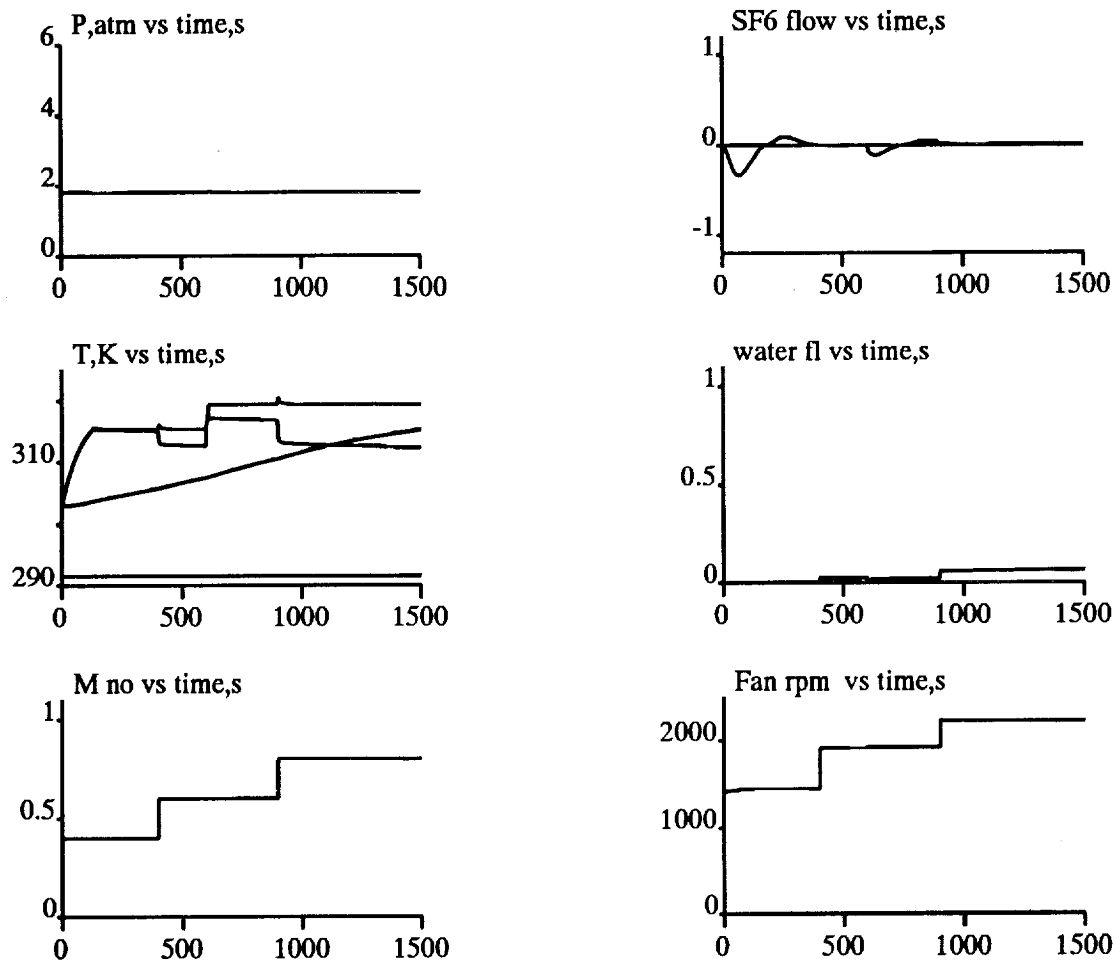

Figure 10i: Simulation of Tunnel Responses

Initial conditions : P=1.8 atm, T=303 K, M=0.4
Set points : P=1.8 atm, T=315.4 K at start & 319.4 K at 600 s
M= 0.6 at 400 s and 0.8 at 900 s
Temperature plots show in descending order Gas, Metal wall(exponential)
Exit water & Sump water (291.5K) temperatures
Gas valves correspond to + for charging & – for recovery
Valves correspond to 0 for close and 1 for full open

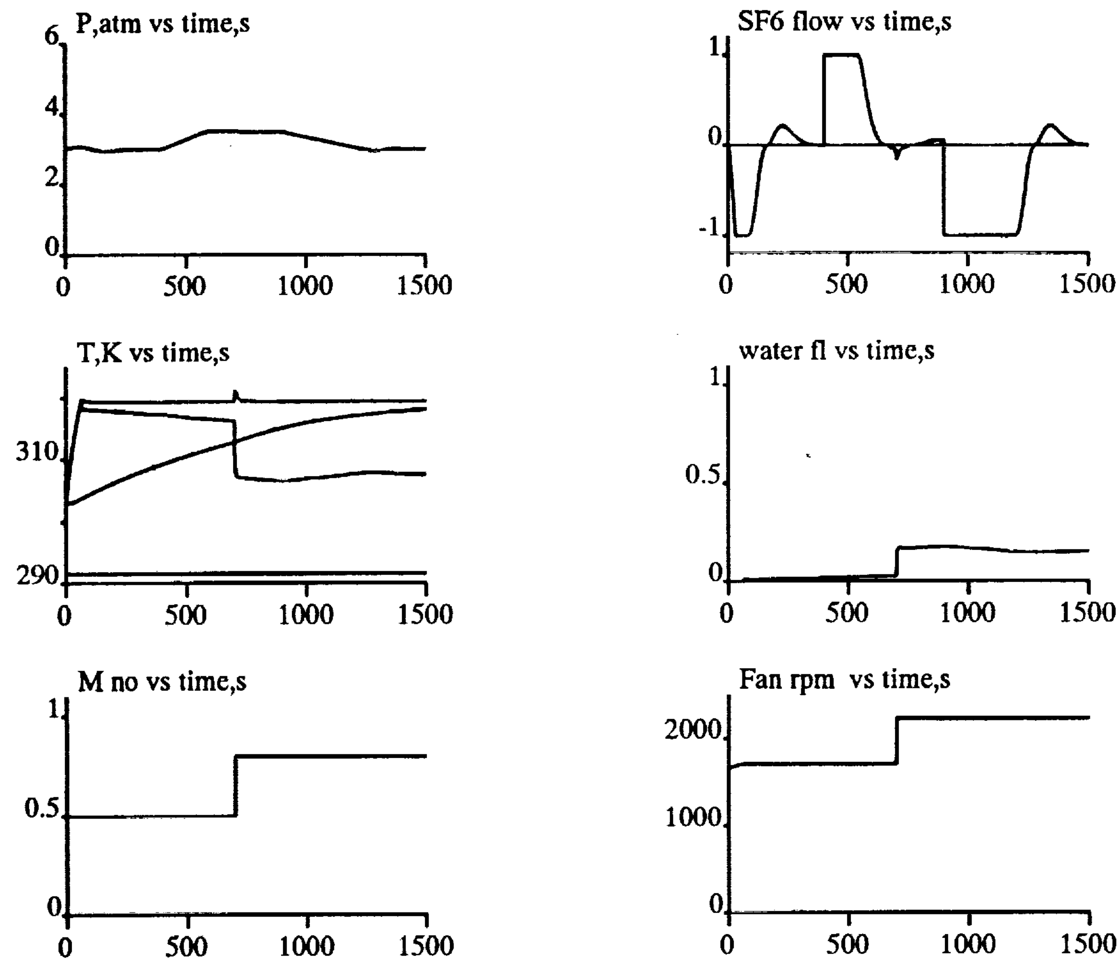

Figure 10j: Simulation of Tunnel Responses

Initial conditions : P=3 atm, T=303 K, M=0.5
Set points : P=3.5 atm at 400 s & 3 atm at 900 s, T=319.4 K
M= 0.8 at 700 s
Temperature plots show in descending order Gas, Metal wall(exponential)
Exit water & Sump water (291.5K) temperatures
Gas valves correspond to + for charging & − for recovery
Valves correspond to 0 for close and 1 for full open

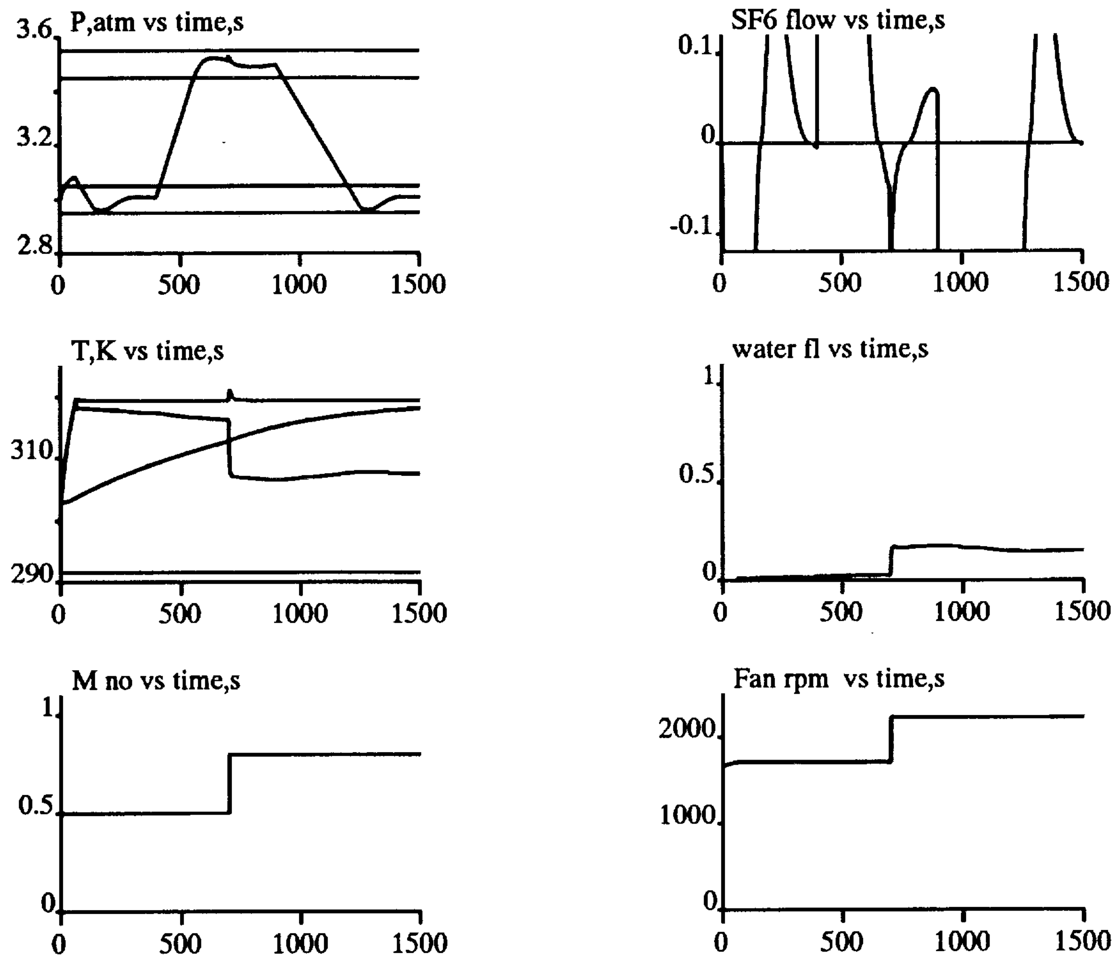

Figure 10k: Simulation of Tunnel Responses (enlarge pressure & gas valve scales)

Initial conditions : P=3 atm, T=303 K, M=0.5
Set points : P=3.5 atm at 400 s & 3 atm at 900 s, T=319.4 K
M= 0.8 at 700 s
Temperature plots show in descending order Gas, Metal wall(exponential)
Exit water & Sump water (291.5K) temperatures
Gas valves correspond to + for charging & − for recovery
Valves correspond to 0 for close and 1 for full open

SF6 P/T/M CONTROLLER

	SF6 PRESSURE / RE NO LOOP AUTO	TEMP LOOP AUTO	RPM/MACH LOOP AUTO
SET POINT	31.10,Psia ,Miln/chrd	319.4,K	0.678,Mach ,RPM
PROCESS	31.10,Psia 24.50,Psia-Static 8.64,Miln/06.00in 98.0% Pure	319.3,K gas 291.0,K Wt-in 312.3,K Wt-out 319.2,K,Wall	0.678,Mach 2081.,RPM
COMMAND	5.3 % opn 0.0 Chrg#3914 Rec#3900	4.7,% opn V1 Wat #344	27.7 ,% Rhst
INPUTS Delete	Psia= APv%= Chrd= Vent= ReNo=	Temp= AWv%=	Mach= Nrpm=
STATUS	SF6sup=280,psig Vac= 2,pisa DelP=0.44,psi Tank=342,psig		Fan pwr=136.8,KW

Figure 11. Controller Display.

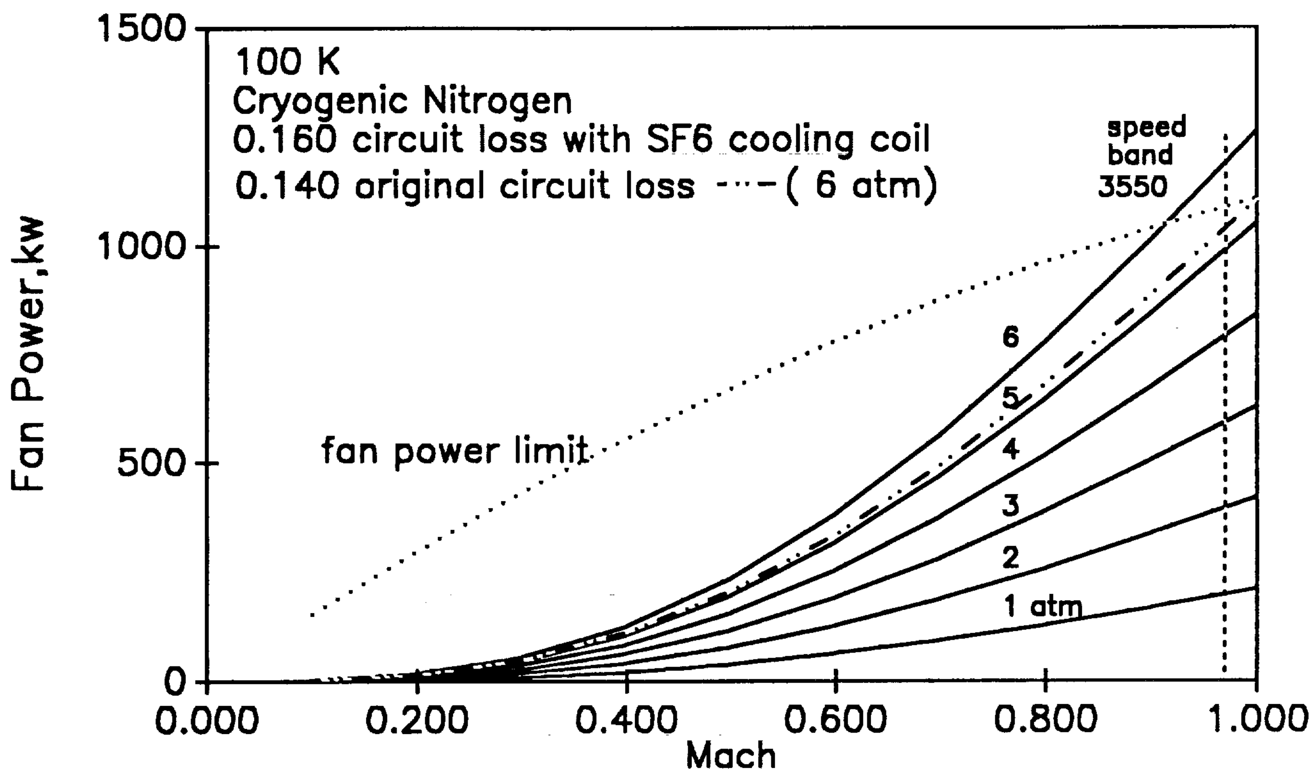

Figure A1:Estimated performance of 0.3–m TCT in nitrogen mode with SF6 mode heat exchanger in the tunnel circuit

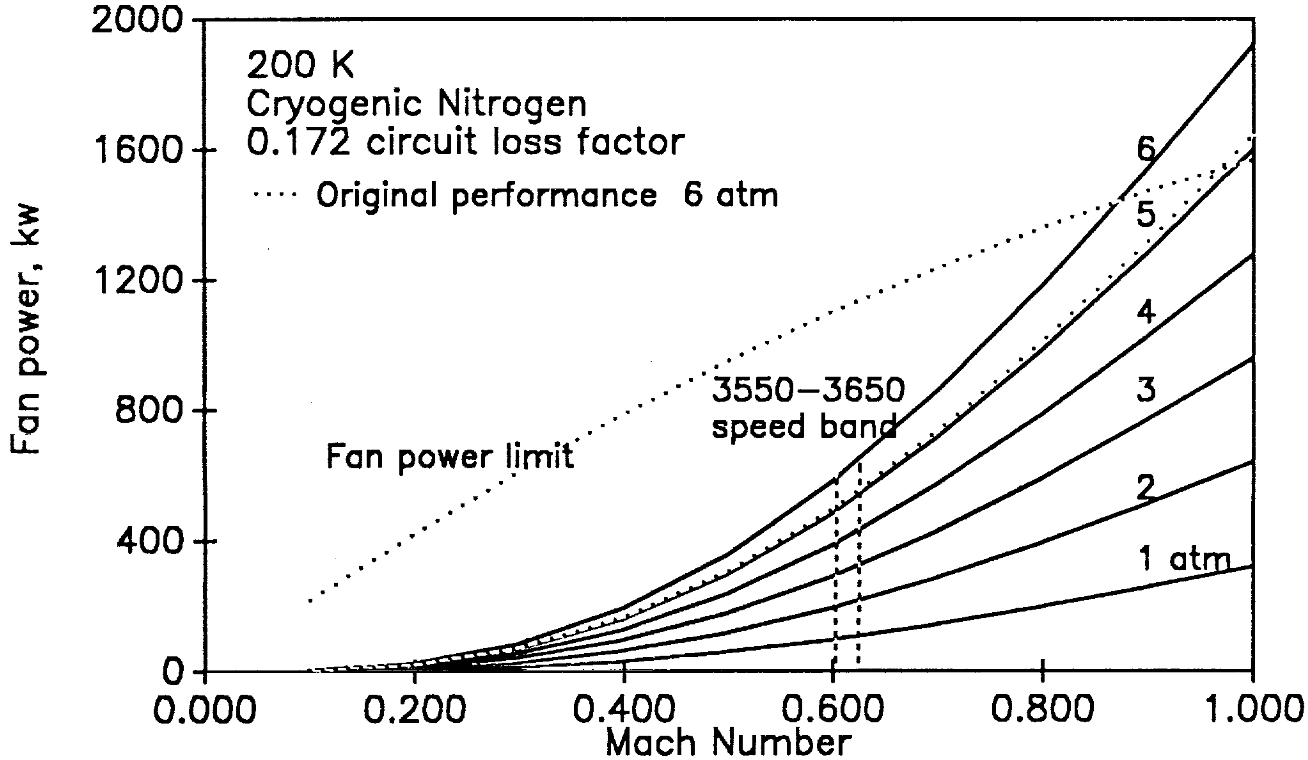

Figure A2: Estimated Performance of 0.3–m TCT in nitrogen mode with heat exchanger in the tunnel circuit

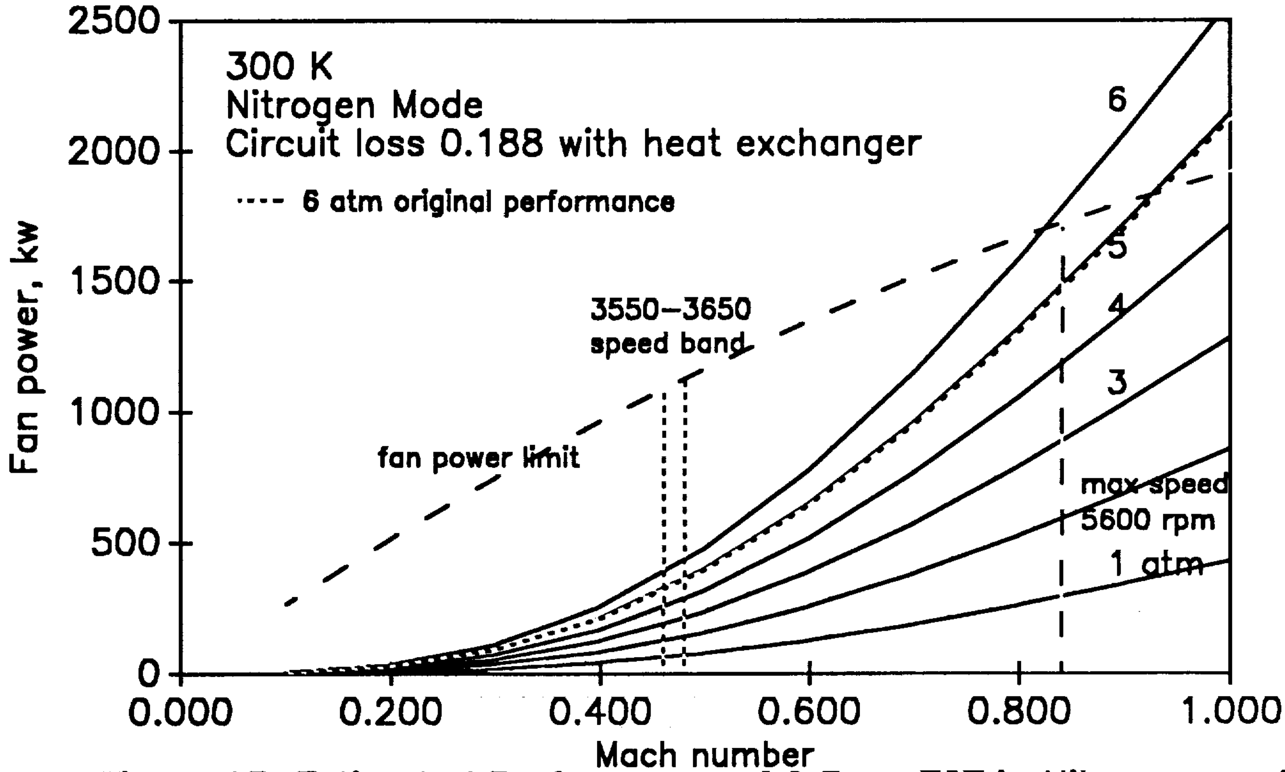

Figure A3: Estimated Performance of 0.3–m TCT in Nitrogen mode with heat exchanger in the tunnel circuit

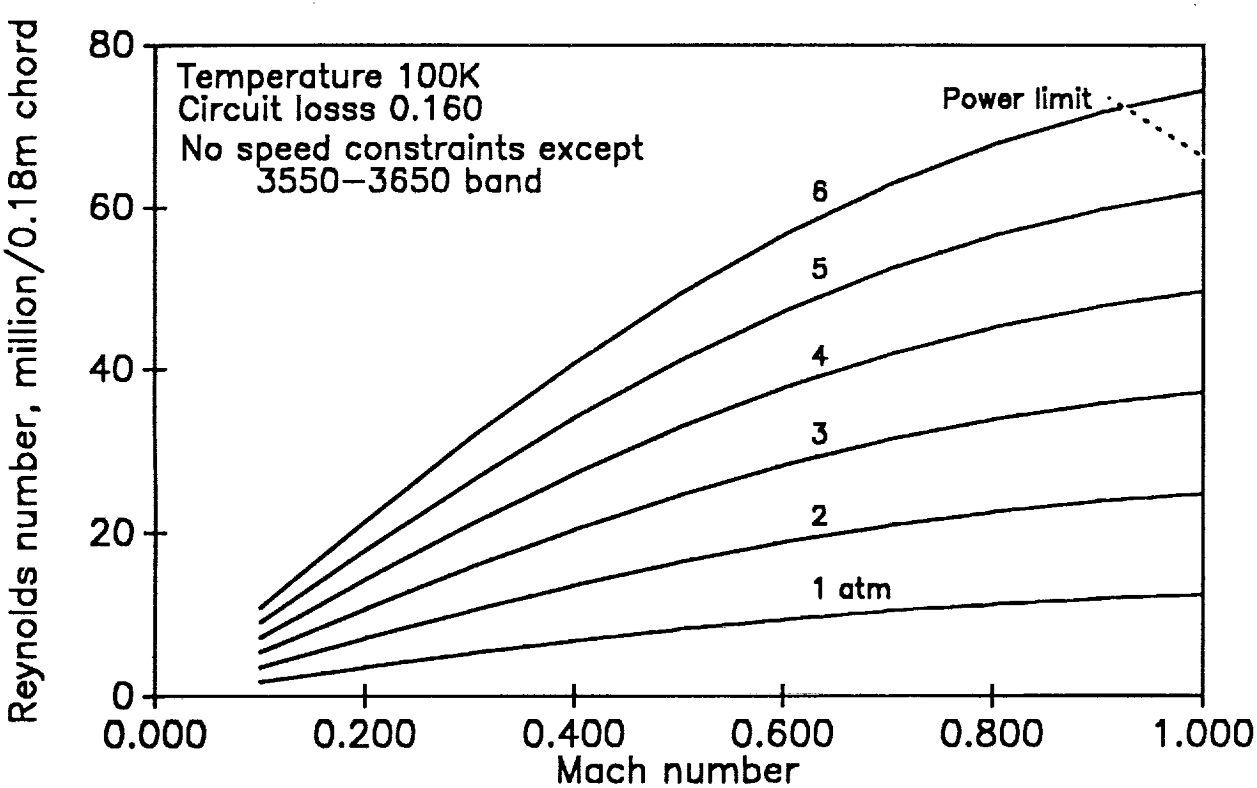

Figure A4: Performance envelope of 0.3–m TCT in nitrogen mode
With SF6 mode heat exchanger in the tunnel circuit

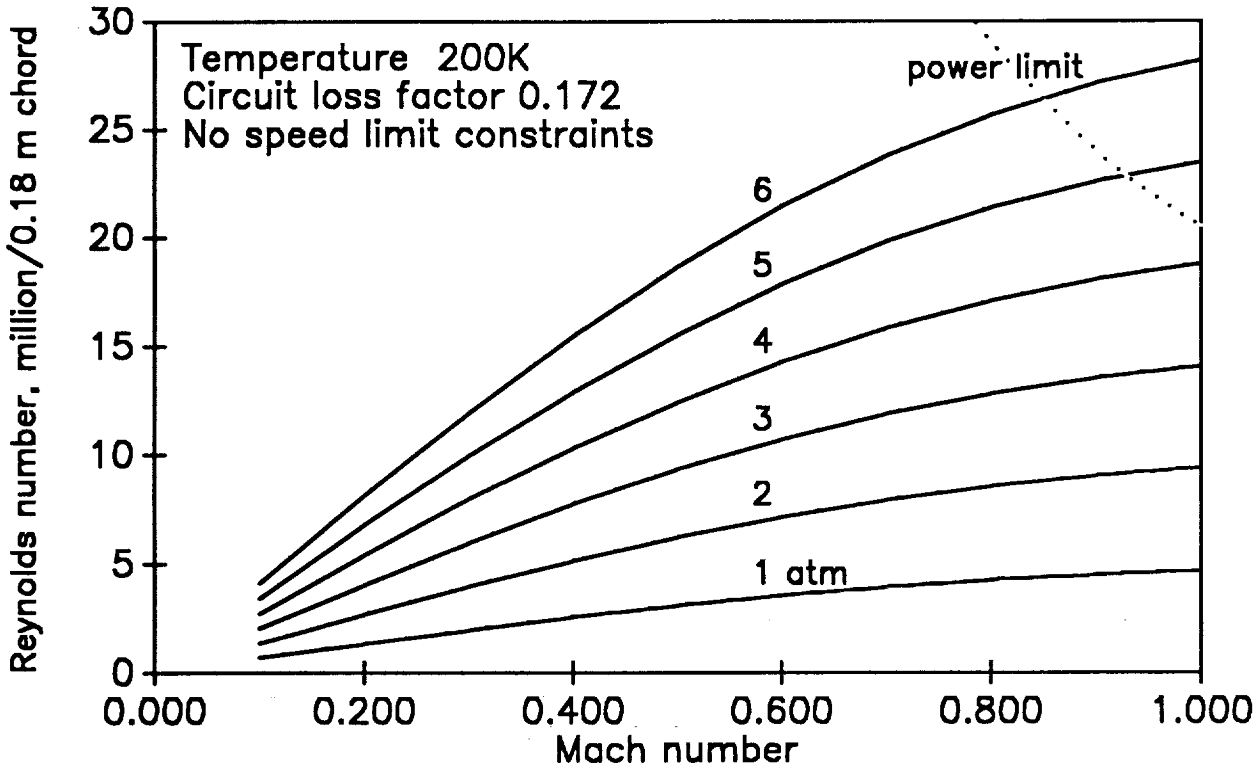

Figure A5: Performance envelope of 0.3−m TCT in nitrogen mode with heat exchanger in the tunnel circuit

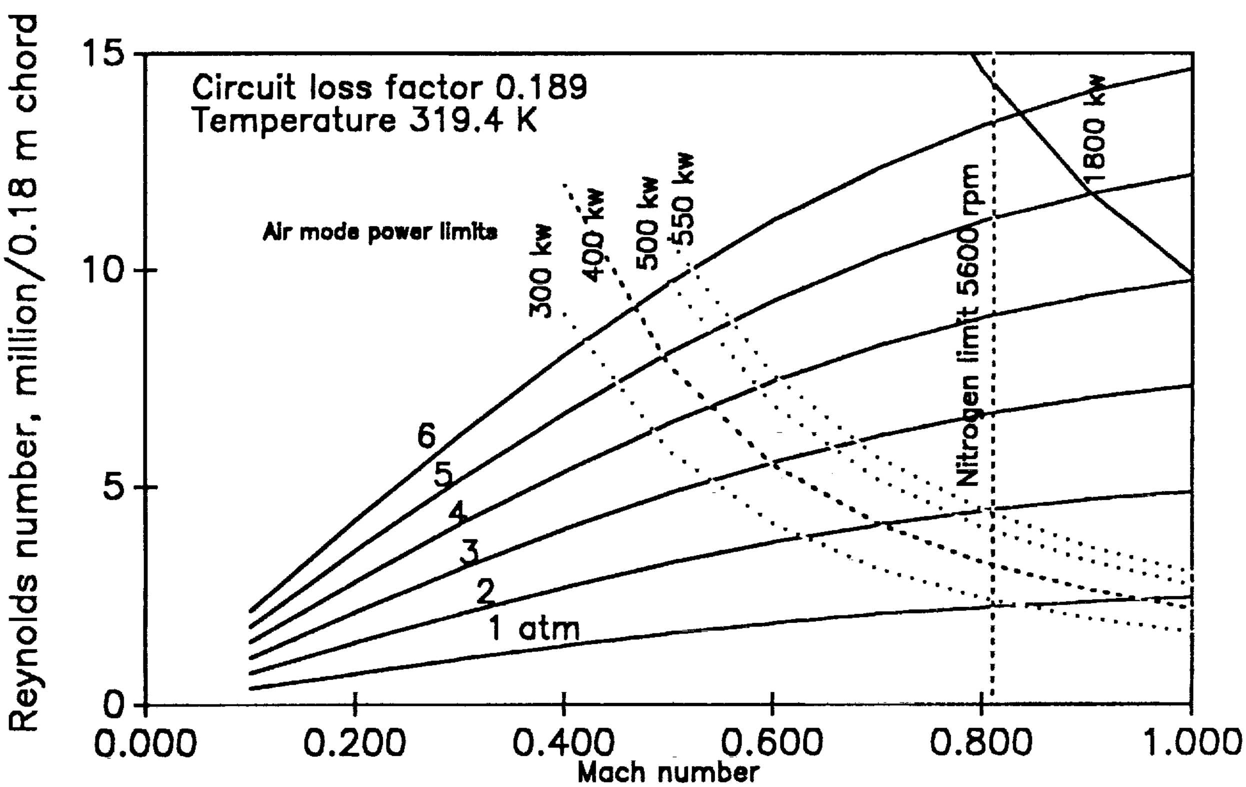

Figure A6: Performance of 0.3–m TCT in Air & Nitrogen with Heat Exchanger in the tunnel circuit

REPORT DOCUMENTATION PAGE

Form Approved
OMB No. 0704-0188

1. AGENCY USE ONLY *(Leave blank)*

2. REPORT DATE
December 1992

3. REPORT TYPE AND DATES COVERED
Contractor Report

4. TITLE AND SUBTITLE
Modeling and Control Study of the NASA 0.3-Meter Transonic Cryogenic Tunnel for Use With Sulfur Hexaflouride Medium

5. FUNDING NUMBERS
C NAS1-18585 Task 77
WU 505-59-86-02

6. AUTHOR(S)
S.Balakrishna and W.Allen Kilgore

7. PERFORMING ORGANIZATION NAME(S) AND ADDRESS(ES)
VIGYAN, Inc.
30 Research Drive, Hampton, Va 23666

8. PERFORMING ORGANIZATION REPORT NUMBER

9. SPONSORING/MONITORING AGENCY NAME(S) AND ADDRESS(ES)
National Aeronautics and Space Administration
Langley Research Center
Hampton, Virginia 23681-0001

10. SPONSORING/MONITORING AGENCY REPORT NUMBER
NASA CR-189737

11. SUPPLEMENTARY NOTES
Langley Technical Monitor: John B. Anders, Jr

12a. DISTRIBUTION/AVAILABILITY STATEMENT
Unclassified - Unlimited

Subject Category 34

12b. DISTRIBUTION CODE

13. ABSTRACT *(Maximum 200 words)*

The NASA Langley 0.3-m Transonic Cryogenic Tunnel is to be modified to operate with sulfur hexafloride gas while retaining its present capability to operate with nitrogen. The modified tunnel will provide high Reynolds number flow on aerodynamic models with two different test gases. The document details a study of the SF6 tunnel performance boundaries, thermodynamic modeling of the tunnel process, nonlinear dynamical simulation of math model to yield tunnel responses, the closed loop control requirements, control laws, and mechanization of the control laws on the microprocessor based controller.

14. SUBJECT TERMS
High Reynolds Number, Heavy gas wind tunnel, tunnel control, tunnel performance

15. NUMBER OF PAGES
61

16. PRICE CODE
A04

17. SECURITY CLASSIFICATION OF REPORT	18. SECURITY CLASSIFICATION OF THIS PAGE	19. SECURITY CLASSIFICATION OF ABSTRACT	20. LIMITATION OF ABSTRACT
Unclassified	Unclassified	Unclassified	

NSN 7540-01-280-5500

Standard Form 298 (Rev. 2-89)
Prescribed by ANSI Std. Z39-18
298-102